Accounts

Phase Transitions in Soft Matter Induced by Selective Solvation

Akira Onuki,* Ryuichi Okamoto, and Takeaki Araki

Department of Physics, Kyoto University, Kyoto 606-8502

Received January 11, 2011; E-mail: onuki@scphys.kyoto-u.ac.jp

We review our recent studies on selective solvation effects in phase separation in polar binary mixtures with a small amount of solutes. Such hydrophilic or hydrophobic particles are preferentially attracted to one of the solvent components. We discuss the role of antagonistic salt composed of hydrophilic and hydrophobic ions, which undergo microphase separation at water–oil interfaces leading to mesophases. We then discuss phase separation induced by a strong selective solvent above a critical solute density n_p, which occurs far from the solvent coexistence curve. We also give theories of ionic surfactant systems and weakly ionized polyelectrolytes including solvation among charged particles and polar molecules. We point out that the Gibbs formula for the surface tension needs to include an electrostatic contribution in the presence of an electric double layer.

1. Introduction

In soft matter physics, much attention has been paid to the consequences of the Coulombic interaction among charged objects, such as small ions, charged colloids, charged gels, and polyelectrolytes.[1–6] However, not enough effort has been made on solvation effects among solutes (including hydrophobic particles) and polar solvent molecules.[7–10] Solvation is also called hydration for water and for aqueous mixtures. In mixtures of a water-like fluid and a less polar fluid (including polymer solutions), the solvation is preferential or selective, depending on whether the solute is hydrophilic or hydrophobic. See Figure 1 for its illustration. The typical solvation free energy much exceeds the thermal energy k_BT per solute particle. Hence selective solvation should strongly influence phase behavior or even induce a new phase transition. In experiments on aqueous mixtures, it is well known that a small amount of salt drastically alters phase behavior.[11–17] In biology, preferential interactions between water and cosolvents with proteins are of crutial importance.[18,19] Thus selective solvation is relevant in diverse fields, but its understanding from physics is still in its infancy.

Around 1980, Nabutovskii et al.[20,21] proposed a possibility of mesophases in electrolytes from a coupling between the composition and the charge density in the free energy. In aqueous mixtures, such a coupling originates from the selective solvation.[22,23] It is in many cases very strong, as suggested by data of the Gibbs transfer free energy in electrochemistry (see Section **2**). Recently, several theoretical groups have proposed Ginzburg–Landau theories on the solvation in mixture solvents for electrolytes,[22–32] polyelectrolytes,[33,34] and ionic surfactants.[35] In soft matter physics, such coarse-grained approaches have been used to understand cooperative effects on mesoscopic scales,[5,6,36] though they are inaccurate on the angstrom scale. They are even more usuful when selective solvation comes into play in the strong coupling limit. This review presents such examples found in our recent research.

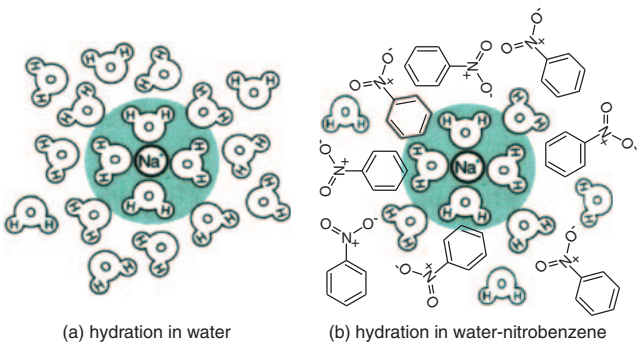

Figure 1. Illustration of hydration of Na^+ surrounded by a shell composed of water molecules in (a) pure water and (b) water–nitrobenzene. The solvation chemical potential of Na^+ is higher for (b) than for (a).

1.1 Antagonistic Salt. An antagonistic salt consists of hydrophilic and hydrophobic ions. An example is sodium tetraphenylborate $NaBPh_4$, which dissociates into hydrophilic Na^+ and hydrophobic BPh_4^-. The latter ion consists of four phenyl rings bonded to an ionized boron. Such ion pairs in aqueous mixtures behave antagonistically in the presence of composition heterogeneity. (i) Around a water–oil interface, they undergo microphase separation on the scale of the Debye screening length κ^{-1}, while homogeneity holds far from the

Published on the web June 4, 2011; doi:10.1246/bcsj.20110012

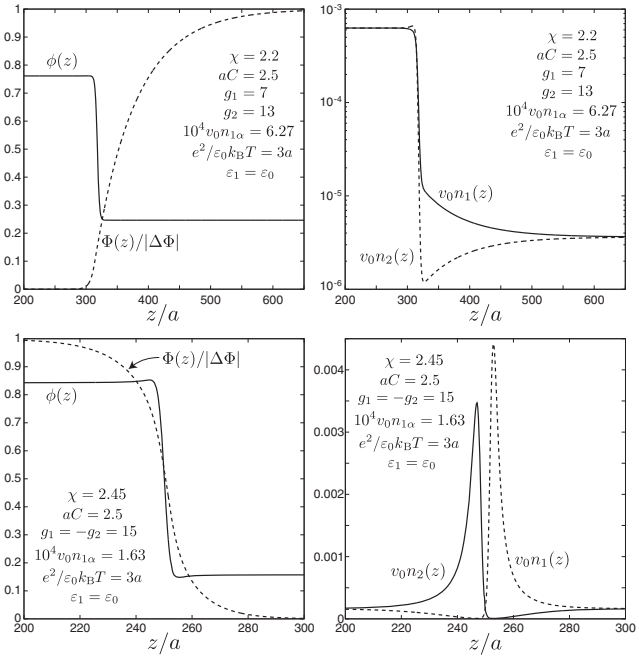

Figure 2. Top: normalized potential $\Phi(z)/\Delta\Phi$ (left), composition $\phi(z)$ (left), and normalized ion densities $v_0 n_1(z)$ and $v_0 n_2(z)$ (right on a semilogarithmic scale) for hydrophilic ion pairs, where $\chi = 2.2$, $g_1 = 7$, $g_2 = 13$, $v_0 n_{1\alpha} = v_0 n_{1\beta} = 4 \times 10^{-4}$, and $e\Delta\Phi = -1.55 k_B T$. Bottom: those for antagonistic ion pairs, where $\chi = 2.45$, $g_1 = 15$, $g_2 = -15$, $v_0 n_{1\alpha} = v_0 n_{1\beta} = 1.63 \times 10^{-4}$, and $e\Delta\Phi = 10.3 k_B T$. In these cases $e^2/\varepsilon_0 k_B T = 3a$ and $\varepsilon_1 = \varepsilon_0$.

interface to satisfy the charge neutrality (see the right bottom plate in Figure 2). This unique ion distribution produces a large electric double layer and a large Galvani potential difference.[23,24,29,30] We found that this ion distribution serves to much decrease the surface tension,[24] in agreement with experiments.[37,38] From X-ray reflectivity measurements, Luo et al.[38] determined such ion distributions around a water–nitrobenzene (NB) interface by adding BPh_4^- and two species of hydrophilic ions. (ii) In the vicinity of the solvent criticality, antagonistic ion pairs interact differently with water-rich and oil-rich composition fluctuations, leading to mesophases (charge density waves). In accord with this prediction, Sadakane et al.[39,40] added a small amount of $NaBPh_4$ to a near-critical mixture of D_2O and 3-methylpyridine (3MP) to find a peak at an intermediate wavenumber q_m ($\approx 0.1\,\text{Å}^{-1} \approx \kappa$) in the intensity of small-angle neutron scattering. The peak height was much enhanced with formation of periodic structures. (iii) Moreover, Sadakane et al. observed multilamellar (onion) structures at small volume fractions of 3MP (in D_2O-rich solvent) far from the criticality,[41] where BPh_4^- and solvating 3MP form charged lamellae. These findings demonstrate very strong hydrophobicity of BPh_4^-. (iv) Another interesting phenomenon is spontaneous emulsification (formation of small water droplets) at a water–NB interface.[42,43] It was observed when a large pure water droplet was pushed into a cell containing NB and antagonistic salt (tetraalkylammonium chloride). This instability was caused by ion transport through the interface.

1.2 Precipitation due to Selective Solvation. Many experimental groups have detected large-scale, long-lived heterogeneities (aggregates or domains) emerging with addition of a hydrophilic salt or a hydrophobic solute in one-phase states of aqueous mixtures.[44–50] Their small diffusion constants indicate that their typical size is of order 10^3 Å at very small volume fractions. In two-phase states, they also observed a third phase visible as a thin solid-like plate at a liquid–liquid interface in two-phase states.[51] In our recent theory,[32] for sufficiently strong solvation preference, a selective solute can induce formation of domains rich in the selected component even very far from the solvent coexistence curve. This phenomenon occurs when the volume fraction of the selected component is relatively small. If it is a majority component, its aggregation is not needed. This precipitation phenomenon should be widely observable for various combinations of solutes and mixture solvents.

1.3 Selective Hydrogen Bonding. Hydrogen bonding is of primary importance in the phase behavior of soft matter. In particular, using statistical–mechanical theories, the origin of closed-loop coexistence curves was ascribed to the hydrogen bonding for liquid mixtures[52,53] and for polymer solutions.[54,55] Interestingly, water itself can be a selective solute triggering phase separation when the hydrogen bonding differs significantly between the two components, as observed in a mixture of methanol–cyclohexane.[56,57] More drastically, even water absorbed from air changed the phase behavior in films of polystyrene (PS)–poly(vinyl methyl ether) (PVME).[58] That is, a small amount of water induces precipitation of PVME-rich domains. For block copolymers, similar precipitation of micelles can well be expected when a small amount of water is added.

1.4 Ionic Surfactant. Surfactant molecules are strongly trapped at an interface due to the amphiphilic interaction even if their bulk density is very low.[6,59] They can thus efficiently reduce the surface tension, giving rise to various mesoscopic structures. However, most theoretical studies have treated nonionic surfactants, while ionic surfactants are important in biology and technology. In this review, we also discuss selective solvation in systems of ionic surfactants, counter ions, and added ions in water–oil.[35] We shall see that the adsorption behavior strongly depends on the selective solvation.

1.5 Polyelectrolytes. Polyelectrolytes are already very complex because of the electrostatic interaction among charged particles (ionized monomers and mobile ions).[2–4] Furthermore, we should take into account two ingredients,[33] which have not yet attracted enough attention. First, the dissociation (or ionization) on the chains should be treated as a chemical reaction in many polyelectrolytes containing weak acidic monomers.[60–62] Then the degree of ionization is a space-dependent annealed variable. Second, the solvation effects should come into play because the solvent molecules and the charged particles interact via ion–dipole interaction. Many polymers themselves are hydrophobic and become hydrophilic with progress of ionization in water. This is because the decrease of the free energy upon ionization is very large. It is also worth noting that the selective solvation effect can be dramatic in mixture solvents.[34] As an example, precipitation of DNA has been observed with addition of ethanol in water,[63–65]

where the ethanol added is excluded from condensed DNA, suggesting solvation-induced wetting of DNA by water. In polyelectrolyte solutions, macroscopic phase separation and mesophase formation can both take place, sensitively depending on many parameters.

The organization of this paper is as follows. In Section **2**, we will present the background of the solvation on the basis of some experiments. In Section **3**, we will explain a Ginzburg–Landau model for electrolytes accounting for selective solvation. In Section **4**, we will treat ionic surfactants by introducing the amphiphilic interaction together with the solvation interaction. In Section **5**, we will examine precipitation induced by a strong selective solute, where a simulation of the precipitation dynamics will also be presented. In Section **6**, we will give a Ginzburg–Landau model for weakly ionized polyelectrolytes accounting for the ionization fluctuations and the solvation interaction. In Appendix A, we will give a statistical theory of hydrophilic solvation at small water contents in oil.

2. Background of Selective Solvation of Ions

2.1 Hydrophilic Ions in Aqueous Mixtures. Several water molecules form a solvation shell surrounding a small ion via ion–dipole interaction,[7] as in Figure 1. Cluster structures produced by solvation have been observed by mass spectrometric analysis.[66,67] Here we mention an experiment by Osakai et al.,[68] which demonstrated the presence of a solvation shell in a water–NB mixture in two-phase coexistence. They measured the amount of water extracted together with hydrophilic ions in a NB-rich region coexisting with a salted water-rich region. A water content of 0.168 M (the water volume fraction ϕ being 0.003) was already present in the NB-rich phase without ions. They estimated the average number of solvating water molecules in the NB-rich phase to be 4 for Na^+, 6 for Li^+, and 15 for Ca^{2+} per ion. Thus, when a hydrophilic ion moves from a water-rich region to an oil-rich region across an interface, a considerable fraction of water molecules solvating it remain attached to it. Furthermore, using proton NMR spectroscopy, Osakai et al.[69] studied successive formation of complex structures of anions X^- (such as Cl^- and Br^-) and water molecules by gradually increasing the water content in NB. This hydration reaction is schematically written as $X^-(H_2O)_{m-1} + H_2O \rightleftarrows X^-(H_2O)_m$ $(m = 1, 2, 3, \ldots)$. For Br^-, these clusters are appreciable for water content larger than 0.1 M or for water volume fraction ϕ exceeding 0.002.

In Appendix A, we will calculate the statistical distribution of clusters composed of ions and polar molecules. Let the free energy typically decrease by ϵ_{bi} upon binding of a polar molecule to a hydrophilic ion of species i. A well-defined solvation shell is formed for $\epsilon_{bi} \gg k_BT$, where the water volume fraction ϕ needs to satisfy

$$\phi > \phi^i_{sol} \approx \exp(-\epsilon_{bi}/k_BT) \tag{2.1}$$

For $\phi \ll \phi^i_{sol}$ there is almost no solvation. The crossover volume fraction ϕ^i_{sol} is very small for strongly hydrophilic ions with $\epsilon_{bi} \gg k_BT$. For Br^- in water–NB, we estimate $\phi^i_{sol} \approx 0.002$ from the experiment by Osakai et al. as discussed above.[69]

2.2 Hydrophobic Particles. Hydrophobic objects are ubiquitous in nature, which repel water because of the strong attraction among hydrogen-bonded water molecules themselves.[7,10] Hydrophobic particles tend to form aggregates in water[70,71] and are more soluble in oil than in water. They can be either neutral or charged. A widely used hydrophobic anion is BPh_4^-. In water, a large hydrophobic particle ($\gtrsim$1 nm) is even in a cavity separating the particle surface from water.[10] In a water–oil mixture, on the other hand, hydrophobic particles should be in contact with oil molecules instead. This attraction can produce significant composition heterogeneities on mesoscopic scales around hydrophobic objects, which indeed takes place around protein surfaces.[18,19]

2.3 Solvation Chemical Potential. We introduce a solvation chemical potential $\mu^i_{sol}(\phi)$ in the dilute limit of solute species i. It is the solvation part of the chemical potential of one particle (see eq B1 in Appendix B). It is a statistical average over the thermal fluctuations of the molecular configurations. In mixture solvents, it depends on the ambient water volume fraction ϕ. For planar surfaces or large particles (such as proteins), we may consider the solvation free energy per unit area.

Born[72] calculated the polarization energy of a polar fluid around a hydrophilic ion with charge Z_ie using continuum electrostatics to obtain the classic formula,

$$(\mu^i_{sol})_{Bom} = -(Z_i^2e^2/2R_i)(1 - 1/\varepsilon) \tag{2.2}$$

The contribution without polarization ($\varepsilon = 1$) or in vacuum is subtracted and the ϕ dependence here arises from that of the dielectric constant $\varepsilon = \varepsilon(\phi)$ (see eq 3.5 below). The lower cutoff R_i is called the Born radius, which is on the order of 1 Å for small metallic ions.[7,73] The hydrophilic solvation is stronger for smaller ions, since it arises from the ion–dipole interaction. In this original formula, neglected are the formation of a solvation shell, the density and composition changes (electrostriction), and the nonlinear dielectric effect.

For mixture solvents, the binding free energy between a hydrophilic ion and a polar molecule is estimated from the Born formula (eq 1) as $\epsilon_{bi} \approx -\partial[(\mu^i_{sol})_{Born}]/\partial\phi$ or[22]

$$\epsilon_{bi} \approx Z_i^2e^2\varepsilon_1/R_i\varepsilon^2 = k_BTZ_i^2\ell_B\varepsilon_1/R_i\varepsilon \tag{2.3}$$

where $\varepsilon_1 = \partial\varepsilon/\partial\phi$ and $\ell_B = e^2/k_BT\varepsilon$ is the Bjerrum length ($\approx$7 Å for water at room temperatures). For $\varepsilon_1 \approx \varepsilon$, a well-defined shell appears for $Z_i^2\ell_B \gg R_i$. The solvation chemical potential $\mu^i_{sol}(\phi)$ of hydrophilic ions in water–oil should largely decrease to negative values in the narrow range $0 < \phi < \phi^i_{sol}$, as will be described in Appendix A. In the wide composition range (eq 2.1), its composition dependence is still very strong such that $|\partial\mu^i_{sol}/\partial\phi| \gg k_BT$ holds (see the next subsection). The solubility of hydrophilic ions should also increase abruptly in the narrow range $\phi < \phi^i_{sol}$ with addition of water to oil. Therefore, solubility measurements of hydrophilic ions would be informative at very small water contents in oil.

In sharp contrast, μ^i_{sol} of a neutral hydrophobic particle increases with increasing the particle radius R in water.[10] It is roughly proportional to the surface area $4\pi R^2$ for $R \gtrsim 1$ nm and is estimated to be about $100k_BT$ at $R \approx 1$ nm. In water–oil solvents, on the other hand, it is not easy to estimate the ϕ dependence of μ^i_{sol}. However, μ^i_{sol} should strongly increase with increasing the water composition ϕ, since hydrophobic particles (including ions) effectively attract oil molecules.[19,41]

2.4 Gibbs Transfer Free Energy. We consider a liquid–liquid interface between a polar (water-rich) phase α and a less polar (oil-rich) phase β with bulk compositions ϕ_α and ϕ_β with $\phi_\alpha > \phi_\beta$. The solvation chemical potential $\mu^i_{\rm sol}(\phi)$ takes different values in the two phases due to its composition dependence. So we define

$$\Delta\mu^i_{\alpha\beta} = \mu^i_{\rm sol}(\phi_\beta) - \mu^i_{\rm sol}(\phi_\alpha) \tag{2.4}$$

In electrochemistry,[68,74–77] the difference of the solvation free energies between two coexisting phases is called the standard Gibbs transfer free energy denoted by $\Delta G^i_{\alpha\beta}$ for each ion species i. Since it is usually measured in units of kJ per mole, its division by the Avogadro number $N_{\rm A}$ gives our $\Delta\mu^i_{\alpha\beta}$ or $\Delta\mu^i_{\alpha\beta} = \Delta G^i_{\alpha\beta}/N_{\rm A}$. With α being the water-rich phase, $\Delta\mu^i_{\alpha\beta}$ is positive for hydrophilic ions and is negative for hydrophobic ions from its definition (eq 2.4). See Appendix B for relations between $\Delta\mu^i_{\alpha\beta}$ and other interface quantities.

For ions, most data of $\Delta G^i_{\alpha\beta}$ are at present limited on water–NB[68,75,76] and water–1,2-dichloroethane (EDC)[77] at room temperatures, where the dielectric constant of NB ($\approx$35) is larger than that of EDC ($\approx$10). They then yield the ratio $\Delta\mu^i_{\alpha\beta}/k_{\rm B}T$. In the case of water–NB, it is 13.6 for Na^+, 27.1 for Ca^{2+}, and 11.3 for Br^- as examples of hydrophilic ions, while it is -14.4 for hydrophobic BPh_4^-. In the case of water–EDC, it is 22,7 for Na^+ and 17.5 for Br^-, while it is -14.1 for BPh_4^-. The amplitude $|\Delta\mu^i_{\alpha\beta}|/k_{\rm B}T$ for hydrophilic ions is larger for EDC than for NB and is very large for multivalent ions. Interestingly, $\Delta\mu^i_{\alpha\beta}$ for H^+ (more precisely hydronium ions H_3O^+) assumes positive values close to those for Na^+ in these two mixtures.

In these experiments on ions, a hydration shell should have been formed around hydrophilic ions even in the water-poor phase β (presumably not completely[69]). From eq 2.1 ϕ_β should be exceeding the crossover volume fraction $\phi^i_{\rm sol}$. The data of the Gibbs transfer free energy quantitatively demonstrate very strong selective solvation even in the range eq 2.1 or after the shell formation.

On the other hand, neutral hydrophobic particles are less soluble in a water-rich phase α than in an oil-rich phase β. Their chemical potential is given by $\mu_i = k_{\rm B}T\ln(n_i{\lambda_i}^3) + \mu^i_{\rm sol}(\phi)$, where i represents the particle species and λ_i is the thermal de Broglie wavelength. From homogeneity of μ_i across an interface, we obtain the ratio of their equilibrium bulk densities as

$$n_{i\beta}/n_{i\alpha} = \exp[-\Delta\mu^i_{\alpha\beta}/k_{\rm B}T] \tag{2.5}$$

where $\Delta\mu^i_{\alpha\beta} < 0$ from the definition (eq 2.4).

3. Ginzburg–Landau Theory of Mixture Electrolytes

3.1 Electrostatic and Solvation Interactions. We present a Ginzburg–Landau free energy F for a polar binary mixture (water–oil) containing a small amount of a monovalent salt ($Z_1 = 1$, $Z_2 = -1$). The multivalent case should be studied separately. The ions are dilute and their volume fractions are negligible, so we are allowed to neglect the formation of ion clusters.[1,78,79] The variables ϕ, n_1, and n_2 are coarse-grained ones varying smoothly on the molecular scale. For simplicity, we also neglect the image interaction.[80,81] At a water–air interface the image interaction serves to push ions into the water region. However, hydrophilic ions are already strongly depleted from an interface due to their position-dependent hydration.[81] See our previous analysis[23] for relative importance between the image interaction and the solvation interaction at a liquid–liquid interface.

The free energy F is the space integral of the free energy density of the form,

$$F = \int {\rm d}\boldsymbol{r}\left[f_{\rm tot} + \frac{1}{2}C|\nabla\phi|^2 + \frac{\varepsilon}{8\pi}\boldsymbol{E}^2\right] \tag{3.1}$$

The first term $f_{\rm tot}$ depends on ϕ, n_1, and n_2 as

$$f_{\rm tot} = f(\phi) + k_{\rm B}T\sum_i n_i\left[\ln(n_i{\lambda_i}^3) - 1 - g_i\phi\right] \tag{3.2}$$

In this paper, the solvent molecular volumes of the two components are assumed to take a common value v_0, though they are often very different in real binary mixtures. Then f is of the Bragg–Williams form,[6,36]

$$\frac{v_0 f}{k_{\rm B}T} = \phi\ln\phi + (1-\phi)\ln(1-\phi) + \chi\phi(1-\phi) \tag{3.3}$$

where χ is the interaction parameter dependent on T. The critical value of χ is 2 without ions. The $\lambda_i = \hbar(2\pi/m_i k_{\rm B}T)^{1/2}$ in eq 3.2 is the thermal de Broglie wavelength of the species i with m_i being the molecular mass. The g_1 and g_2 are the solvation coupling constants. In addition, the coefficient C in the gradient part of eq 3.1 remains an arbitrary constant. To explain experiments, however, it is desirable to determine C from the surface tension data or from the scattering data.

In the electrostatic part of eq 3.1, the electric field is written as $\boldsymbol{E} = -\nabla\Phi$. The electric potential Φ satisfies the Poisson equation,

$$-\nabla\cdot\varepsilon\nabla\Phi = 4\pi\rho \tag{3.4}$$

The dielectric constant ε is assumed to depend on ϕ as

$$\varepsilon(\phi) = \varepsilon_0 + \varepsilon_1\phi \tag{3.5}$$

where ε_0 and ε_1 are positive constants. Though there is no reliable theory of $\varepsilon(\phi)$ for a polar mixture, a linear composition dependence of $\varepsilon(\phi)$ was observed by Debye and Kleboth for a mixture of nitrobenzene–2,2,4-trimethylpentane.[82] In addition, the form of the electrostatic part of the free energy density depends on the experimental method.[83] Our form in eq 3.1 follows if we insert the fluid between parallel plates and fix the charge densities on the two plate surfaces.

We explain the solvation terms in $f_{\rm tot}$ in more detail. They follow if $\mu^i_{\rm sol}(\phi)$ ($i = 1, 2$) depend on ϕ linearly as

$$\mu^i_{\rm sol}(\phi) = A_i - k_{\rm B}Tg_i\phi \tag{3.6}$$

Here the first term A_i is a constant yielding a contribution linear with respect to n_i in $f_{\rm tot}$, so it is irrelevant at constant ion numbers. The second term in eq 3.6 gives rise to the solvation coupling in $f_{\rm tot}$. In this approximation, $g_i > 0$ for hydrophilic ions and $g_i < 0$ for hydrophobic ions. The difference of the solvation chemical potentials in two-phase coexistence in eq 2.4 is given by

$$\Delta\mu^i_{\rm sol} = k_{\rm B}Tg_i\Delta\phi \tag{3.7}$$

where $\Delta\phi = \phi_\alpha - \phi_\beta$ is the composition difference. From eqs B4 and B5, the Galvani potential difference is

$$\Delta\Phi = k_B T(g_1 - g_2)\Delta\phi/2e \tag{3.8}$$

and the ion reduction factor is

$$n_{1\beta}/n_{1\alpha} = n_{2\beta}/n_{2\alpha} = \exp[-(g_1 + g_2)\Delta\phi/2] \tag{3.9}$$

The discussion in Subsection **2.3** indicates $g_i \approx 14$ (23) for Na^+ ions and $g_i \approx -14$ (-14) for BPh_4^- in water–NB (water–EDC) at 300 K. For multivalent ions g_i can be very large ($g_i \approx 27$ for Ca^{2+} in water–NB). The linear form (eq 3.6) is adopted for the mathematical simplicity and is valid for $\phi > \phi^i_{sol}$ after the solvation shell formation (see eq 2.1). The results in Appendix A suggest a more complicated functional form of $\mu^i_{sol}(\phi)$.

In equilibrium, we require the homogeneity of the chemical potentials $h = \delta F/\delta\phi$ and $\mu_i = \delta F/\delta n_i$. Here,

$$h = f' - C\nabla^2\phi - \frac{\varepsilon_1}{8\pi}\boldsymbol{E}^2 - k_B T\sum_i g_i n_i \tag{3.10}$$

$$\mu_i = k_B T[\ln(n_i {\lambda_i}^3) - g_i\phi] + Z_i e\Phi \tag{3.11}$$

where $f' = \partial f/\partial\phi$. The ion distributions are expressed in terms of ϕ and Φ in the modified Poisson–Boltzmann relations,[23]

$$n_i = n_i^0 \exp[g_i\phi - Z_i e\Phi/k_B T] \tag{3.12}$$

The coefficients n_i^0 are determined from the conservation of the ion numbers, $\langle n_i\rangle = V^{-1}\int d\boldsymbol{r} n_i(\boldsymbol{r}) = n_0$, where $\langle\cdots\rangle = V^{-1}\int d\boldsymbol{r}(\cdots)$ denotes the space average with V being the cell volume. The average $n_0 = \langle n_1\rangle = \langle n_2\rangle$ is a given constant density in the monovalent case.

It is worth noting that a similar Ginzburg–Landau free energy was proposed by Aerov et al.[84] for mixtures of ionic and nonionic liquids composed of anions, cations, and water-like molecules. In such mixtures, the interactions among neutral molecules and ions can be preferential, leading to mesophase formation, as has been predicted also by molecular dynamic simulations.[85]

3.2 Structure Factors and Effective Ion–Ion Interaction in One-Phase States. The simplest application of our model is to calculate the structure factors of the the composition and the ion densities in one-phase states. They can be measured by scattering experiments.

We superimpose small deviations $\delta\phi(\boldsymbol{r}) = \phi(\boldsymbol{r}) - \langle\phi\rangle$ and $\delta n_i(\boldsymbol{r}) = n_i(\boldsymbol{r}) - n_0$ on the averages $\langle\phi\rangle$ and n_0. The monovalent case ($Z_1 = 1$, $Z_2 = -1$) is treated. As thermal fluctuations, the statistical distributions of $\delta\phi(\boldsymbol{r})$ and δn_i are Gaussian in the mean field theory. We may neglect the composition-dependence of ε for such small deviations. We calculate the following,

$$S(q) = \langle|\phi_{\boldsymbol{q}}|^2\rangle_e, \quad G_{ij}(q) = \langle n_{i\boldsymbol{q}} n^*_{j\boldsymbol{q}}\rangle_e/n_0,$$
$$C(q) = \langle|\rho_{\boldsymbol{q}}|^2\rangle_e/e^2 n_0 \tag{3.13}$$

where $\phi_{\boldsymbol{q}}$, $n_{i\boldsymbol{q}}$, and $\rho_{\boldsymbol{q}}$ are the Fourier components of $\delta\phi$, δn_i, and the charge density $\rho = e(n_1 - n_2)$ with wave vector $\boldsymbol{q}$ and $\langle\cdots\rangle_e$ denotes taking the thermal average. We introduce the Bjerrum length $\ell_B = e^2/\varepsilon k_B T$ and the Debye wavenumber $\kappa = (8\pi\ell_B n_0)^{1/2}$.

First, the inverse of $S(q)$ is written as[22,23]

$$\frac{1}{S(q)} = \bar{r} - (g_1 + g_2)^2\frac{n_0}{2} + \frac{Cq^2}{k_B T}\left[1 - \frac{\gamma_p^2\kappa^2}{q^2 + \kappa^2}\right] \tag{3.14}$$

where $\bar{r} = f''/k_B T$ with $f'' = \partial^2 f/\partial\phi^2$. The second term is large for large $(g_1 + g_2)^2$ even for small average ion density n_0, giving rise to a large shift of the spinodal curve. If $g_1 \approx g_2 \approx 15$, this factor is of order 10^3. In the previous experiments,[11–17] the shift of the coexistence curve is typically a few Kelvins with addition of a 10^{-3} mole fraction of a hydrophilic salt like NaCl. The parameter γ_p in the third term represents asymmetry of the solvation of the two ion species and is defined by

$$\gamma_p = (k_B T/16\pi C\ell_B)^{1/2}|g_1 - g_2| \tag{3.15}$$

If the right hand side of eq 3.14 is expanded with respect to q^2, the coefficient of q^2 is $C(1 - \gamma_p^2)/k_B T$. Thus a Lifshitz point is realized at $\gamma_p = 1$. For $\gamma_p > 1$, $S(q)$ has a peak at an intermediate wavenumber,

$$q_m = (\gamma_p - 1)^{1/2}\kappa \tag{3.16}$$

The peak height $S(q_m)$ and the long wavelength limit $S(0)$ are related by

$$1/S(q_m) = 1/S(0) - C(\gamma_p - 1)^2\kappa^2/k_B T \tag{3.17}$$

A mesophase appears with decreasing $\bar{r}$ or increasing χ, as observed by Sadakane et al.[39] In our mean-field theory, the criticality of a binary mixture disappears if a salt with $\gamma_p > 1$ is added however small its content is. Very close to the solvent criticality, Sadakane et al.[40] recently measured anomalous scattering from D_2O–3MP–$NaBPh_4$ stronger than that from D_2O–3MP without $NaBPh_4$. There, the observed scattering amplitude is not well described by the mean-field $S(q)$ in eq 3.14, requiring more improvement.

Second, retaining the fluctuations of the ion densities, we eliminate the composition fluctuations in F to obtain the effective interactions among the ions mediated by the composition fluctuations. The resultant free energy of ions is written as[23]

$$F_{ion} = \int d\boldsymbol{r}\sum_i k_B T n_i \ln(n_i {\lambda_i}^3) + \frac{1}{2}\int d\boldsymbol{r}\int d\boldsymbol{r}'\sum_{i,j} V_{ij}(|\boldsymbol{r} - \boldsymbol{r}'|)\delta n_i(\boldsymbol{r})\delta n_j(\boldsymbol{r}') \tag{3.18}$$

The effective interaction potentials $V_{ij}(r)$ are given by

$$V_{ij}(r) = Z_i Z_j\frac{e^2}{\varepsilon r} - \frac{g_i g_j}{A}\frac{1}{r}e^{-r/\xi} \tag{3.19}$$

where Z_1 and Z_2 are ± 1 in the monovalent case, $A = 4\pi C/(k_B T)^2$, and $\xi = (C/\bar{r})^{1/2}$ is the correlation length without ions. The second term in eq 3.19 arises from the selective solvation and is effective in the range $a \lesssim r \lesssim \xi$ and can be increasingly important on approaching the solvent criticality (for $\xi \gg a$). It is attractive among the ions of the same species ($i = j$) dominating over the Coulomb repulsion for

$$g_i^2 > 4\pi C\ell_B/k_B T \tag{3.20}$$

Under the above condition there should be a tendency of ion aggregation of the same species. In the antagonistic case ($g_1 g_2 < 0$), the cations and anions can repel one another in the range $a \lesssim r \lesssim \xi$ for

$$|g_1 g_2| > 4\pi C\ell_B/k_B T \tag{3.21}$$

under which charge density waves are triggered near the solvent criticality.

The ionic structure factors can readily be calculated from eqs 3.18 and 3.19. Some calculations give[30]

$$\frac{G_{ii}(q)}{G_0(q)} = 1 + n_0 S(q)\frac{[(g_1+g_2)(u+1/2)-g_i u]^2}{G_0(q)(u+1)^2},$$
$$2G_{12}(q) = \frac{1}{u+1} + n_0 S(q)\left[\frac{(g_1+g_2)^2}{2} - \frac{(g_1-g_2)^2u^2}{2(u+1)^2}\right],$$
$$C(q) = \frac{2u}{u+1} + n_0 S(q)\frac{(g_1-g_2)^2}{(u+1)^2}u^2 \quad (3.22)$$

where $u = q^2/\kappa^2$ and

$$G_0(q) = \frac{u+1/2}{u+1} = \frac{q^2+\kappa^2/2}{q^2+\kappa^2} \quad (3.23)$$

is the structure factor for the cations (or for the anions) divided by n_0 in the absence of solvation. The solvation parts in eq 3.22 are all proportional to $n_0S(q)$, where $S(q)$ is given by eq 3.14. The Coulomb interaction suppresses large-scale charge-density fluctuations, so $C(q)$ tends to zero as $q \to 0$.

It should be noted that de Gennes[86] derived the effective interaction among monomers on a chain ($\propto -e^{-r/\xi}/r$) mediated by the composition fluctuations in a mixture solvent. He then predicted anomalous size behavior of a chain near the solvent criticality. However, as shown in eq 3.19, the effective interaction is much more amplified among charged particles than among neutral particles. This indicates importance of the selective solvation for a charged polymer in a mixture solvent, even leading to a prewetting transition around a chain.[34] We also point out that an attractive interaction arises among charged colloid particles due to the selective solvation in a mixture solvent, on which we will report shortly.

3.3 Liquid–Liquid Interface Profiles. The second application is to calculate a one-dimensional liquid–liquid interface at $z = z_0$ taking the z axis in its normal direction, where $\phi \to \phi_\alpha$ in water-rich phase α ($z - z_0 \to -\infty$) and $\phi \to \phi_\beta$ in oil-rich phase β ($z - z_0 \to \infty$). In Figure 2, we give numerical results of typical interface profiles, where we measure space in units of $a \equiv {v_0}^{1/3}$ and set $C = 2.5k_BT/a^2$, $e^2/\varepsilon_0 k_B T = 3a$, and $\varepsilon_1 = \varepsilon_0$. In these examples, the correlation length ξ is shorter than the Debye lengths ${\kappa_\alpha}^{-1}$ and ${\kappa_\beta}^{-1}$ in the two phases. However, near the solvent criticality, ξ grows above ${\kappa_\alpha}^{-1}$ and ${\kappa_\beta}^{-1}$ and we encounter another regime, which is not treated in this review.

The upper plates give $\phi(z)$, $\Phi(z)$, $n_1(z)$, and $n_2(z)$ for hydrophilic ion pairs with $g_1 = 7$ and $g_2 = 13$ at $\chi = 2.2$ and $n_{1\alpha} = n_{2\alpha} = 4 \times 10^{-4}{v_0}^{-1}$. The ion reduction factor in eq 3.9 is 0.0057. The potential Φ varies mostly in the right side (phase β) on the scale of the Debye length ${\kappa_\beta}^{-1} = 67.5a$ (which is much longer than that ${\kappa_\alpha}^{-1} = 6.1a$ in phase α). The Galvani potential difference $\Delta\Phi$ is $0.76k_BT/e$ here. The surface tension here is $\sigma = 6.53 \times 10^{-2}k_BT/a^2$ and is slightly larger than that $\sigma_0 = 6.22k_BT/a^2$ without ions (see the next subsection).

The lower plates display the same quantities for antagonistic ion pairs with $g_1 = 15$ and $g_2 = -15$ for $\chi = 2.45$ and $n_{1\alpha} = n_{2\alpha} = 1.67 \times 10^{-4}{v_0}^{-1}$. The anions and the cations are undergoing microphase separation at the interface on the scale of the Debye lengths ${\kappa_\alpha}^{-1} = 12.3a$ and ${\kappa_\beta}^{-1} = 9.70a$, resulting in a large electric double layer and a large potential drop ($\approx 10k_BT/e$). The surface tension here is $\sigma = 0.0805k_BT/a^2$ and is about half of that $\sigma_0 = 0.155k_BT/a^2$ without ions. This large decrease in σ is marked in view of small $n_{1\alpha}$. A large decrease of the surface tension was observed for an antagonistic salt.[37,38]

3.4 Surface Tension. There have been numerous measurements of the surface tension of an air–water interface with a salt in the water region. In this case, almost all salts lead to an increase in the surface tension,[80,81] while acids tend to lower it because hydronium ions are trapped at an air–water interface.[87,88]

Here, we consider the surface tension of a liquid–liquid interface in our Ginzburg–Landau scheme, where ions can be present in the two sides of the interface. In equilibrium we minimize $\Omega = \int dz\omega$, where ω is the grand potential density,

$$\omega = f_{tot} + \frac{1}{2}C|\nabla\phi|^2 + \frac{\varepsilon}{8\pi}\boldsymbol{E}^2 - h\phi - \sum_i \mu_i n_i \quad (3.24)$$

Using eqs 3.10 and 3.11 we find $d(\omega + \rho\Phi)/dz = 2C\phi'\phi''$, where $\phi' = d\phi/dz$ and $\phi'' = d^2\phi/dz^2$. Thus,

$$\omega = C\phi'^2 - \rho\Phi + \omega_\infty \quad (3.25)$$

Since ϕ' and ρ tend to zero far from the interface, $\omega(z)$ tends to a common constant ω_∞ as $z \to \pm\infty$. The surface tension $\sigma = \int dz[\omega(z) - \omega_\infty]$ is then written as[23,24]

$$\sigma = \int dz\left[C\phi'^2 - \frac{\varepsilon}{4\pi}\boldsymbol{E}^2\right] = 2\sigma_g - 2\sigma_e \quad (3.26)$$

where we introduce the areal densities of the gradient free energy and the electrostatic energy as

$$\sigma_g = \int dz C\phi'^2/2, \quad \sigma_e = \int dz\varepsilon\boldsymbol{E}^2/8\pi \quad (3.27)$$

The expression $\sigma = 2\sigma_g$ is well-known in the Ginzburg–Landau theory without the electrostatic interaction.[36]

In our previous work,[23,24] we obtained the following approximate expression for σ valid for small ion densities:

$$\sigma \cong \sigma_0 - k_BT\Gamma - \sigma_e \quad (3.28)$$

where σ_0 is the surface tension without ions and Γ is the adsorption to the interface. In terms of the total ion density $n = n_1 + n_2$, it may be expressed as

$$\Gamma = \int dz\left[n - n_\alpha - \frac{\Delta n}{\Delta\phi}(\phi - \phi_\alpha)\right] \quad (3.29)$$

where $n_K = n_{1K} + n_{2K}$ ($K = \alpha, \beta$), $\Delta n = n_\alpha - n_\beta$, and the integrand tends to zero as $z \to \pm\infty$. From eqs 3.26 and 3.28 σ_g is expressed at small ion densities as

$$2\sigma_g \cong \sigma_0 - k_BT\Gamma + \sigma_e \quad (3.30)$$

In the Gibbs formula ($\sigma \cong \sigma_0 - k_BT\Gamma$),[6,89] the electrostatic contribution $-\sigma_e$ is neglected. However, it is crucial for antagonistic salt[24,29] and for ionic surfactant.[35]

In Figure 3, numerical results of $2\sigma_e$, $2\sigma_g$, σ, and the combination $\sigma_0 - k_BT\Gamma + \sigma_e$ are plotted as functions of the bulk ion density $n_\alpha = n_{1\alpha} + n_{2\alpha}$ for the antagonistic case $g_1 = -g_2 = 15$, where $\chi = 2.4$ and $C = 2.5k_BT/a^2$. The parameter γ_p in eq 3.15 exceeds unity (being equal to 1.89 for $\varepsilon = 1.5\varepsilon_0$). In this example, σ_g weakly depends on n_α and is

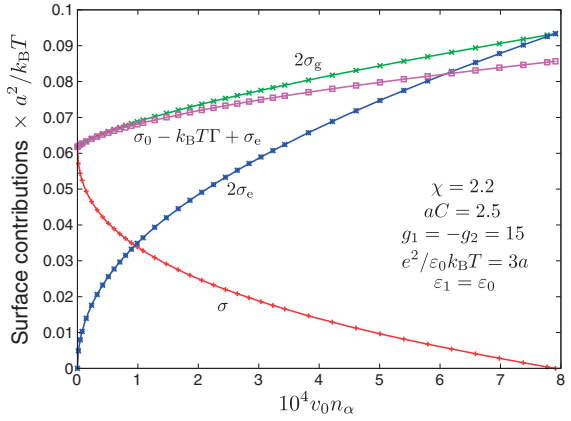

Figure 3. Surface quantities σ, $2\sigma_e$, $2\sigma_g$, and $\sigma_0 - k_BT\Gamma + \sigma_e$ in units of k_BTa^{-2} vs. v_0n_α for a monovalent, antagonistic salt with $g_1 = -g_2 = 15$ at $\chi = 2.4$. Here $2\sigma_g$ and $\sigma_0 - k_BT\Gamma + \sigma_e$ are close, supporting eq 3.30. Growth of $2\sigma_e$ gives rise to vanishing of the surface tension σ at $v_0n_\alpha = 8 \times 10^{-4}$.

fairly in accord with eq 3.30, while σ_e steeply increases with increasing n_α. As a result, σ_e increases up to σ_g, leading to vanishing of σ at $n_\alpha \cong 8 \times 10^{-4}v_0^{-1}$.

We may understand the behavior of σ_e as a function of g_1 and g_2 by solving the nonlinear Poisson–Boltzmann eq,[24] with an interface at $z = 0$. That is, away from the interface $|z| > \xi$, the normalized potential $U(z) \equiv e\Phi(z)/k_BT$ obeys

$$\frac{d^2}{dz^2}U = \kappa_K{}^2 \sinh(U - U_K) \tag{3.31}$$

in the two phases ($K = \alpha$, β), where $U_\alpha = U(-\infty)$, $U_\beta = U(\infty)$, and $\kappa_K = (4\pi n_K e^2/\varepsilon_K k_BT)^{1/2}$ with $\varepsilon_K = \varepsilon_0 + \varepsilon_1\phi_K$. In solving eq 3.31 we assume the continuity of the electric induction $-\varepsilon d\Phi/dz$ at $z = 0$ (but this does not hold in the presence of interfacial orientation of molecular dipoles, as will be remarked in the summary section). The Poisson–Boltzmann approximation for σ_e is of the form,

$$\frac{\sigma_e^{PB}}{k_BT} = \frac{2n_\alpha}{\kappa_\alpha}\left[\sqrt{1 + b^2 + 2b\cosh(\Delta U/2)} - b - 1\right]$$
$$= A_s(n_\alpha/\ell_{B\alpha})^{1/2} \tag{3.32}$$

We should have $\sigma_e \cong \sigma_e^{PB}$ in the thin interface limit $\xi \ll \kappa_K{}^{-1}$. In the first line, the coefficient b is defined by

$$b = (\varepsilon_\beta/\varepsilon_\alpha)^{1/2}\exp[-(g_1 + g_2)\Delta\phi/4] \tag{3.33}$$

and $\Delta U = U_\alpha - U_\beta = (g_1 - g_2)\Delta\phi/2$ is the normalized potential difference calculated from eq 3.8. In the second line, $\ell_{B\alpha} = e^2/\varepsilon_\alpha k_BT$ is the Bjerrum length in phase α. The second line indicates that the electrostatic contribution to the surface tension is negative and is of order $n_\alpha{}^{1/2}$ as $n_\alpha \to 0$ away from the solvent criticality, as first predicted by Nichols and Pratt for liquid–liquid interfaces.[90] Remarkably, the surface tension of air–water interfaces exhibited the same behavior at very small salt densities (known as the Jones–Ray effect),[91] though it has not yet been explained reliably.[24]

In the asymptotic limit of antagonistic ion pairs, we assume $g_1 \geq -g_2 \gg 1$, where the coefficient A_s in the second line of eq 3.32 grows as

$$A_s \cong \pi^{-1/2}(\varepsilon_\beta/\varepsilon_\alpha)^{1/4}\exp(|g_2|\Delta\phi/4) \tag{3.34}$$

We may also examine the usual case of hydrophilic ion pairs in water–oil, where g_1 and g_2 are both considerably larger than unity. In this case A_s becomes small as

$$A_s \cong (\varepsilon_\beta/\pi\varepsilon_\alpha)^{1/2}[\cosh(\Delta U/2) - 1]$$
$$\times \exp[-(g_1 + g_2)\Delta\phi/4] \tag{3.35}$$

In this case, the electrostatic contribution $-\sigma_e(\propto n_\alpha{}^{1/2})$ in σ could be detected only at extremely small salt densities.

Analogously, between ionic and nonionic liquids, Aerov et al.[84] calculated the surface tension. They showed that if the affinities of cations and anions to neutral molecules are very different, the surface tension becomes negative.

3.5 Mesophase Formation with Antagonistic Salt. Adding an antagonistic salt with $\gamma_p > 1$ to water–oil, we have found instability of one-phase states with increasing χ below eq 3.15 and vanishing of the surface tension σ with increasing the ion content as in Figure 3. In such cases, a thermodynamic instability is induced with increasing χ at a fixed ion density $n_0 = \langle n_1\rangle = \langle n_2\rangle$, leading to a mesophase. To examine this phase ordering, we performed two-dimensional simulations[29,30] and presented an approximate phase diagram.[30] We here present preliminary three-dimensional results. The patterns to follow resemble those in block copolymers and surfactant systems.[36,92] In our case, mesophases emerge due to the selective solvation and the Coulomb interaction without complex molecular structures. Solvation-induced mesophase formation can well be expected in polyelectrolytes and mixtures of ionic and polar liquids.

We are interested in slow composition evolution with antagonistic ion pairs, so we assume that the ion distributions are given by the modified Poisson–Boltzmann relations in eq 3.12. The water composition ϕ obeys[29,30]

$$\frac{\partial\phi}{\partial t} + \nabla\cdot(\phi\boldsymbol{v}) = \frac{L_0}{k_BT}\nabla^2 h \tag{3.36}$$

where L_0 is the kinetic coefficient and h is defined by eq 3.10. Neglecting the acceleration term, we determine the velocity field $\boldsymbol{v}$ using the Stokes approximation,

$$\eta_0\nabla^2\boldsymbol{v} = \nabla p_1 + \phi\nabla h + \sum_i n_i\nabla\mu_i \tag{3.37}$$

where η_0 is the shear viscosity and μ_i are defined by eq 3.11, We introduce p_1 to ensure the incompressibility condition $\nabla\cdot\underleftrightarrow{\boldsymbol{v}} = 0$. The right hand side of eq 3.37 is also written as $\nabla\cdot\underleftrightarrow{\Pi}$, where $\underleftrightarrow{\Pi}$ is the stress tensor arising from the fluctuations of ϕ and n_i. Here the total free energy F in eq 3.1 satisfies $dF/dt \leq 0$ with these equations (if the boundary effect arising from the surface free energy is neglected).

We integrated eq 3.36 using the relations eqs 3.4, 3.12, and 3.37 on a $64 \times 64 \times 64$ lattice under the periodic boundary condition. The system was quenched to an unstable state with $\chi = 2.1$ at $t = 0$. Space and time are measured in units of $a = v_0{}^{1/3}$ and $t_0 = a^5/L_0$, respectively. Without ions, the diffusion constant of the composition is given by L_0f''/k_BT in one-phase states in the long wavelength limit (eq 3.14). We set $g_1 = -g_2 = 10$, $n_0 = 3 \times 10^{-3}v_0^{-1}$, $C = k_BT/2a^2$, $e^2/\varepsilon_0k_BT = 3a$, $\varepsilon_1 = 0$, and $\eta_0L_0/k_BT = 0.16a^4$.

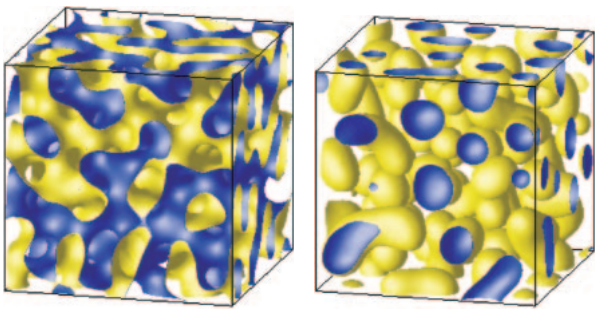

Figure 4. Composition patterns at $t = 5000t_0$ for $\chi = 2.1$ and $v_0\bar{n} = 3 \times 10^{-3}$ with average composition $\langle\phi\rangle$ being 0.5 (left) and 0.4 (right) for antagonistic salt with $g_1 = -g_2 = 10$. These patterns are nearly pinned. Yellow surfaces are oriented to the regions of $\phi > 0.5$ and blue ones are to those of $\phi < 0.5$.

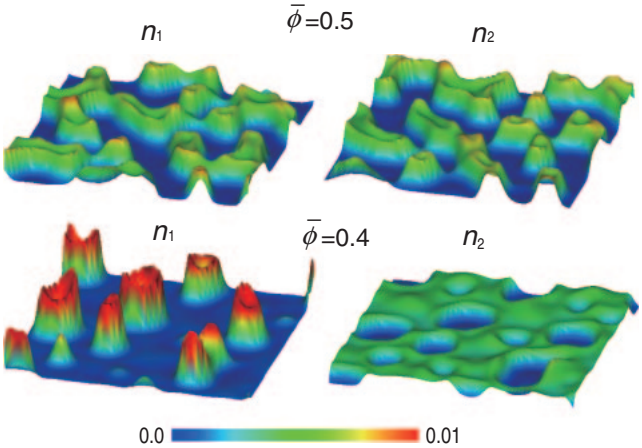

Figure 5. Cross-sectional profiles of cation n_1 (left) and anion n_2 (right) in the x–y plane at $z = 0$ for antagonistic salt using data in Figure 4. The domains are bicontinuous for $\langle\phi\rangle = 0.5$ (top) and droplet-like for $\langle\phi\rangle = 0.4$ (bottom).

In Figure 4, we show the simulated domain patterns at $t = 5000t_0$, where we can see a bicontinuous structure for $\langle\phi\rangle = 0.5$ and a droplet structure for $\langle\phi\rangle = 0.4$. There is almost no further time evolution from this stage. In Figure 5, the ion distributions are displayed for these two cases in the x–y plane at $z = 0$. For $\langle\phi\rangle = 0.5$, the ion distributions are peaked at the interfaces forming electric double layers (as in the right bottom plate of Figure 2). For $\langle\phi\rangle = 0.4$, the anions are broadly distributed in the percolated oil region, but we expect formation of electric double layers with increasing the domain size also in the off-critical condition. In Figure 6, the structure factor $S(q)$ in steady states are plotted for $v_0n_0 = 0.001$, 0.002, and 0.003. The peak position decreases with increasing n_0 in accord with eq 3.16. Sadakane et al.[39,41] observed the structure factor similar to those in Figure 6.

Finally, we remark that the thermal noise, which is absent in our simulation, should be crucial near the criticality of low-molecular-weight solvents. It is needed to explain anomalously enhanced composition fluctuations induced by $NaBPh_4$ near the solvent criticality.[40]

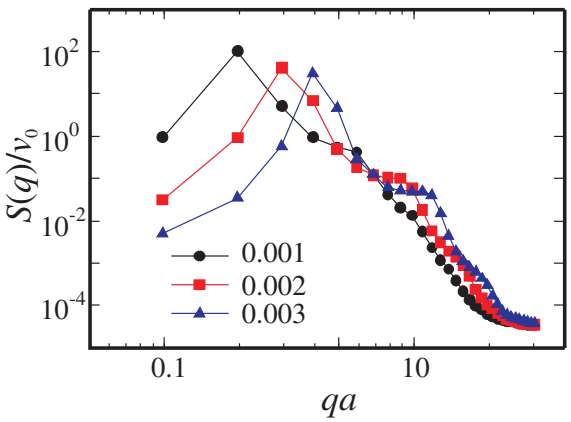

Figure 6. Normalized structure factor $S(q)/v_0$ for antagonistic salt from domain structures in pinned states at $t = 5000t_0$, where the patterns are bicontinuous at for $\langle\phi\rangle = 0.5$. A peak height $S(q_m)/v_0$ of each curve much exceed unity. The average ion density is $v_0n_0 = 0.001$, 0.002, and 0.003 for the three curves (from above for $q < q_m$).

4. Ionic Surfactant with Amphiphilic and Solvation Interactions

4.1 Ginzburg–Landau Theory. In this section, we will give a diffuse-interface model of ionic surfactants,[35] where surfactant molecules are treated as ionized rods. Their two ends can stay in very different environments (water and oil) if they are longer than the interface thickness ξ. In our model, the adsorption of ionic surfactant molecules and counter ions to an oil–water interface strongly depends on the selective solvation parameters g_1 and g_2 and that the surface tension contains the electrostatic contribution as in eqs 3.26 and 3.28.

We add a small amount of cationic surfactant, anionic counter ions in water–oil in the monovalent case. The densities of water, oil, surfactant, and counter ion are n_A, n_B, n_1, and n_2, respectively. The volume fractions of the first three components are $\phi_A = v_0n_A$, $\phi_B = v_0n_B$, and v_1n_1, where v_0 is the common molecular volume of water and oil and v_1 is the surfactant molecular volume. The volume ratio $N_1 = v_1/v_0$ can be large, so we do not neglect the surfactant volume fraction, while we neglect the counter ion volume fraction supposing a small size of the counter ions. We assume the space-filling condition,

$$\phi_A + \phi_B + v_1n_1 = 1 \tag{4.1}$$

Let $2\psi = \phi_A - \phi_B$ be the composition difference between water and oil; then,

$$\begin{aligned}\phi_A &= (1 - v_1n_1)/2 + \psi,\\ \phi_B &= (1 - v_1n_1)/2 - \psi\end{aligned} \tag{4.2}$$

The total free energy F is again expressed as in eq 3.1. Similarly to eq 3.2, the first part reads

$$\begin{aligned}\frac{f_{tot}}{k_BT} = \frac{1}{v_0}[\phi_A \ln\phi_A + \phi_B \ln\phi_B + \chi\phi_A\phi_B]\\ + \sum_i n_i[\ln(n_i\lambda_i^3) - g_in_i\psi] - n_1 \ln Z_a\end{aligned} \tag{4.3}$$

The coefficients g_1 and g_2 are the solvation parameters of the ionic surfactant and the counter ions, respectively. Though a surfactant molecule is amphiphilic, it can have preference to water or oil on the average. The last term represents the amphiphilic interaction between the surfactant and the composition. That is, Z_a is the partition function of a rod-like dipole with its center at the position $\boldsymbol{r}$. We assume that the surfactant molecules take a rod-like shape with a length 2ℓ considerably longer than $a = v_0^{1/3}$. It is given by the following integral on the surface of a sphere with radius ℓ,

$$Z_a(\boldsymbol{r}) = \int \frac{d\Omega}{4\pi} \exp[w_a \psi(\boldsymbol{r} - \ell\boldsymbol{u}) - w_a \psi(\boldsymbol{r} + \ell\boldsymbol{u})] \quad (4.4)$$

where $\boldsymbol{u}$ is the unit vector along the rod direction and $\int d\Omega$ represents the integration over the angles of $\boldsymbol{u}$. The two ends of the rod are at $\boldsymbol{r} + \ell\boldsymbol{u}$ and $\boldsymbol{r} - \ell\boldsymbol{u}$ under the influence of the solvation potentials given by $k_B T w_a \psi(\boldsymbol{r} + \ell\boldsymbol{u})$ and $-k_B T w_a \psi(\boldsymbol{r} - \ell\boldsymbol{u})$. The parameter w_a represents the strength of the amphiphilic interaction.

Adsorption is strong for large $w_a \Delta\psi \gg 1$, where $\Delta\psi = \psi_\alpha - \psi_\beta$ ($\cong \phi_{A\alpha} - \phi_{A\beta}$) is the difference of ψ between the two phases α and β. In the one-dimensional case, all the quantities vary along the z axis and Z_a is rewritten as

$$Z_a(z) = \int_{-\ell}^{\ell} \frac{d\zeta}{2\ell} \exp[w_a \psi(z - \zeta) - w_a \psi(z + \zeta)] \quad (4.5)$$

where $\zeta = \ell u_z$. In the thin interface limit $\xi \ll \ell$, we place the interface at $z = 0$ to find $Z_a = 1$ for $|z| > \ell$, while

$$Z_a(z) \cong 1 + (1 - |z|/\ell)[\cosh(w_a \Delta\psi) - 1] \quad (4.6)$$

for $|z| < \ell$. Furthermore, in the dilute limit $v_1 n_1 \ll 1$ and without the electrostatic interaction, we have $n_1(z) = n_{1\alpha} Z_a(z)$ for $z < 0$ and $n_1(z) = n_{1\beta} Z_a(z)$ for $z > 0$, where $n_{1\alpha}$ and $n_{1\beta} = e^{-g_1 \Delta\psi} n_{1\alpha}$ are the bulk surfactant densities. The surfactant adsorption then grows as

$$\Gamma_1 = \int_{-\infty}^{0} dz[n_1(z) - n_\alpha] + \int_{0}^{\infty} dz[n_1(z) - n_\beta]$$
$$= (n_{1\alpha} + n_{1\beta})\ell[\cosh(w_a \Delta\psi) - 1]/2 \quad (4.7)$$

However, the steric effect comes into play at the interface with increasing the surfactant volume fraction at the interface ($\approx \Gamma_1 v_1/\ell$).

4.2 Interface Profiles of Compositions, Ion Densities, and Potential. We give typical one-dimensional interface profiles varying along the z axis in Figure 7. We set $v_1 = 5v_0$, $C = 3k_B T/a$, $\chi = 3$, and $e^2/a\varepsilon_c k_B T = 16/\pi$. The dielectric constant is assumed to be of the form $\varepsilon = \varepsilon_c(1 + 0.8\psi)$, where ε_c is the critical value. Then $\varepsilon_\alpha \cong 2\varepsilon_\beta$ at $\chi = 3$. This figure was produced in the presence of the image interaction in our previous work[35] (though it is not essential here).

In Figure 7, we show the volume fractions ϕ_A, ϕ_B, and $v_1 n_1 = 1 - \phi_A - \phi_B$ (top), the ion densities n_1 and n_2 (middle), and the potential $e\Phi/k_B T$ with $\Phi_\alpha = 0$ (bottom). In the left, the counter ions are more hydrophilic than the cationic surfactant, where $g_1 = 4$ and $g_2 = 10$ leading to $\Gamma = 0.124a^{-2}$ and $\sigma = 0.317 k_B T a^{-2}$ at $n_{1\alpha} = 10^{-3} v_0^{-1}$. In the right plates, the surfactant cations are hydrophilic and the counter ions are hydrophobic, where $g_1 = -g_2 = 8$ leading to $\Gamma = 0.155a^{-2}$ and $\sigma = 0.159 k_B T a^{-2}$ at $n_{1\alpha} = 3.6 \times 10^{-4} v_0^{-1}$. The distribution

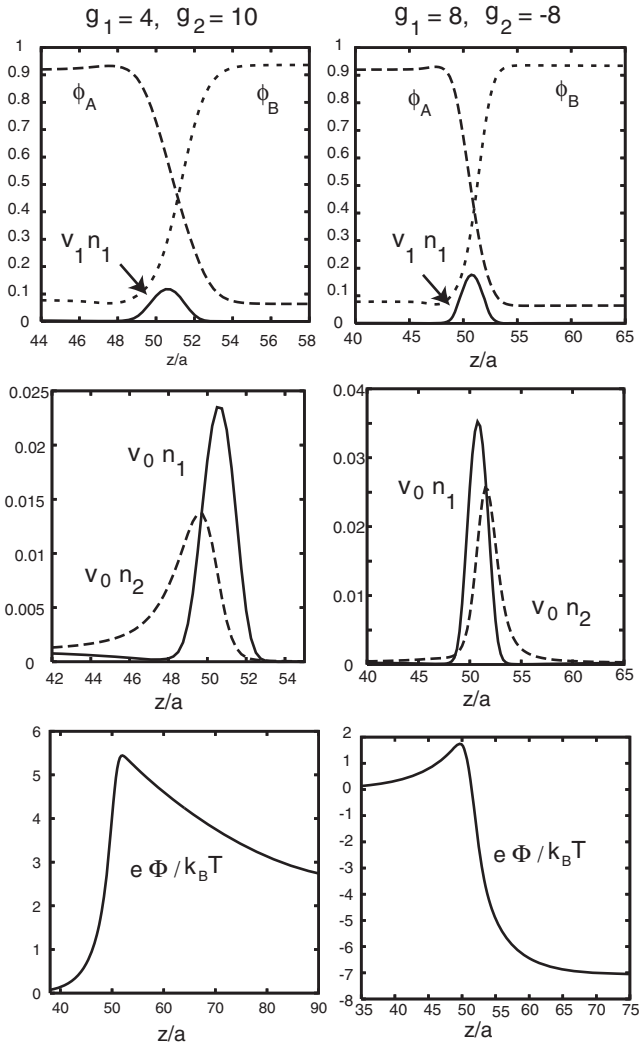

Figure 7. Profiles for mixtures with cationic surfactant and anionic counter ions with $v_1 = 5v_0$ and $w_a = 12$. Top: $v_1 n_1$ (bold line), ϕ_A, and ϕ_B. Middle: $v_0 n_1$ and $v_0 n_2$. Bottom: $e\Phi/k_B T$ exhibiting a maximum at the interface. Here $g_1 = 4$, $g_2 = 10$, and $v_0 n_{1\alpha} = 10^{-3}$ (left), while $g_1 = -g_2 = 8$ and $v_0 n_{1\alpha} = 3.6 \times 10^{-4}$ (right). The counter ion distribution has a peak in the phase α (left) or β (right) depending on g_2 (From: A. Onuki, *Europhys. Lett.* **2008**, *82*, 58002).

of the surfactant n_1 is narrower than that of the counter ions n_2. This gives rise to a peak of Φ at $z = z_p$, at which $E(z_p) \propto \int_{-\infty}^{z_p} dz(n_1(z) - n_2(z)) = 0$.

The adsorption strongly depends on the solvation parameters g_1 and g_2. It is much more enhanced for antagonistic ion pairs than for hydrophilic ion pairs.

4.3 Surface Tension. The grand potential density ω is again given by eq 3.24 and tends to a common constant ω_∞ as $z \to \pm\infty$, though its form is more complicated. The surface tension $\sigma = \int dz[\omega(z) - \omega_\infty]$ is rewritten as eq 3.26 and is approximated as eq 3.28 for small $n_{1\alpha}$. The areal electrostatic-energy density σ_e in eq 3.27 is again important in the present case.

In Figure 8, we show σ, $\sigma + \sigma_e$, and Γ as functions of $v_0 n_{1\alpha}$ at $w_a = 12$, where Γ is defined as in eq 3.28 for $n = n_1 + n_2$. In

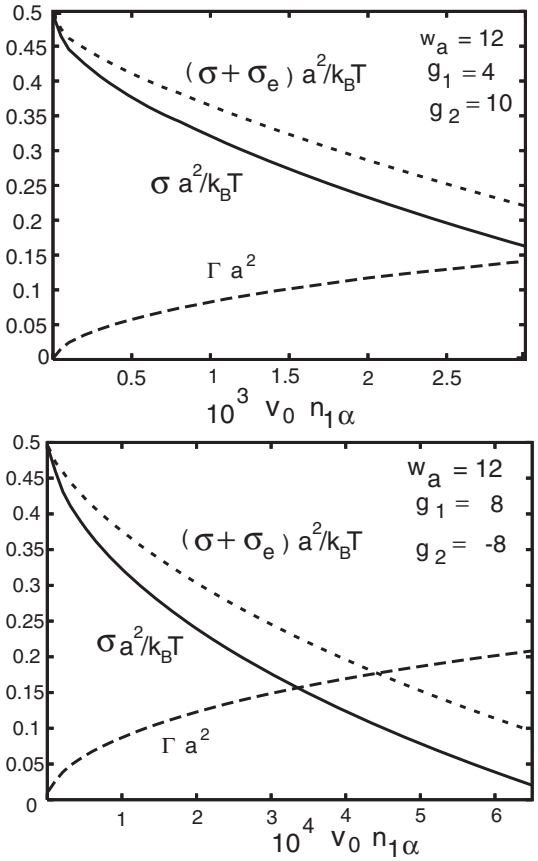

Figure 8. $\sigma a^2/k_BT$, $(\sigma + \sigma_e)a^2/k_BT$, and Γa^2 as functions of $v_0 n_{1\alpha}$ with $v_1 = 5v_0$, $\chi = 3$, and $w_a = 12$. The curves change on a scale of 10^{-3} for hydrophilic ion pair $g_1 = 4$ and $g_2 = 10$ (top) and on a scale of 10^{-4} for antagonistic ion pair $g_1 = -g_2 = 8$ (bottom) (From: A. Onuki, *Europhys. Lett.* **2008**, *82*, 58002).

the upper plate, the two species of ions are both hydrophilic ($g_1 = 4$ and $g_2 = 10$), while in the lower plate the surfactant and the counter ions are antagonistic ($g_1 = 8$ and $g_2 = -8$). For the latter case, a large electric double layer is formed at an interface, leading to a large Γ and a large decrease in σ even at very small n_{1a}. In the present case the Gibbs term $k_BT\Gamma$ is a few times larger than σ_e. Note that the approximate formula (eq 3.28) may be derived also in this case, but it is valid only for very small n_{1a} in Figure 8.

5. Phase Separation due to Strong Selective Solvation

5.1 Strongly Hydrophilic or Hydrophobic Solute. With addition of a strongly selective solute in a binary mixture in one-phase states, we predict precipitation of domains composed of the preferred component enriched with the solute.[32] These precipitation phenomena occur both for a hydrophilic salt (such as NaCl) and a neutral hydrophobic solute.[44–50] In our scheme, a very large size of the selective solvation parameter g_i is essential. In Sections **2** and **3**, we have shown that $|g_i|$ can well exceed 10 both for hydrophilic and hydrophobic solutes.

With hydrophilic cations and anions, a charge density appears only near the interfaces, shifting the surface tension slightly. Thus, in the static aspect of precipitation, the electrostatic interaction is not essential, while fusion of precipitated domains should be suppressed by the presence of the electric double layers. We will first treat a hydrophilic neutral solute as a third component, but the following results are applicable also to a neutral hydrophobic solute if water and oil are exchanged. In addition, in a numerical example in Figure 11, we will include the electrostatic interaction among hydrophilic ions.

5.2 Conditions of Two Phase Coexistence. Adding a small amount of a highly selective solute in water–oil, we assume the following free energy density,

$$f_{\rm tot}(\phi, n) = f(\phi) + k_BTn[\ln(n\lambda^3) - 1 - g\phi] \tag{5.1}$$

This is a general model for a dilute solute. For monovalent electrolytes, this form follows from eq 3.11 if there is no charge density or if we set

$$n_1 = n_2 = n/2, \quad g = (g_1 + g_2)/2 \tag{5.2}$$

The first term $f(\phi)$ is assumed to be of the Bragg–Williams form (eq 3.3). The λ is the thermal de Broglie length. The solvation term ($\propto g$) arises from the solute preference of water over oil (or oil over water). The strength g is assumed to much exceed unity.[23] We fix the amounts of the constituent components in the cell with a volume V. Then the averages $\bar{\phi} = \langle\phi\rangle = \int d\boldsymbol{r}\phi/V$ and $\bar{n} = \langle n\rangle = \int d\boldsymbol{r}n/V$ are given control parameters as well as χ.

In two phase coexistence in equilibrium, let the composition and the solute density be (ϕ_α, n_α) in phase α and (ϕ_β, n_β) in phase β, where $\phi_\alpha > \bar{\phi} > \phi_\beta$ and $n_\alpha > \bar{n} > n_\beta$. We introduce the chemical potentials $h = \partial f_{\rm tot}/\partial\phi$ and $\mu = \partial f_{\rm tot}/\partial n$. Equation 5.1 yields

$$h = f'(\phi) - k_BTgn \tag{5.3}$$

$$\mu/k_BT = \ln(n\lambda^3) - g\phi \tag{5.4}$$

where $f' = \partial f/\phi$. The system is linearly stable for $\partial h/\partial\phi - (\partial h/\partial n)^2/\partial\mu/\partial n > 0$ or for

$$f''(\phi) - k_BTg^2n > 0 \tag{5.5}$$

where $f'' = \partial^2 f/\partial\phi^2$. Spinodal decomposition occurs if the left hand side of eq 5.5 is negative.

The homogeneity of μ yields

$$n = \bar{n}e^{g\phi}/\langle e^{g\phi}\rangle \tag{5.6}$$

where $\langle\cdots\rangle$ denotes taking the space average. The bulk solute densities are $n_K = \bar{n}e^{g\phi_K}/\langle e^{g\phi}\rangle$ for $K = \alpha$, β in two-phase coexistence. In our approximation eq 5.6 holds even in the interface regions. We write the volume fraction of phase α as γ_α. We then have $\langle e^{g\phi}\rangle = \gamma_\alpha e^{g\phi_\alpha} + (1 - \gamma_\alpha)e^{g\phi_\beta}$ in eq 5.6. In terms of $\bar{\phi}$ and $\bar{n}$, γ_α is expressed as

$$\gamma_\alpha = (\bar{\phi} - \phi_\beta)/\Delta\phi = (\bar{n} - n_\beta)/\Delta n \tag{5.7}$$

where $\Delta\phi = \phi_\alpha - \phi_\beta > 0$ and $\Delta n = n_\alpha - n_\beta > 0$. In these expressions we neglect the volume of the interface regions. Since $n_\alpha/n_\beta = e^{g\Delta\phi} \gg 1$ for $g\Delta\phi \gg 1$, the solute is much more enriched in phase α than in phase β. Eliminating n using eq 5.6, we may express the average free energy density as

$$\langle f_{\rm tot}\rangle = \langle f\rangle - k_BT\bar{n}\ln[\langle e^{g\phi}\rangle] + A_1 \tag{5.8}$$

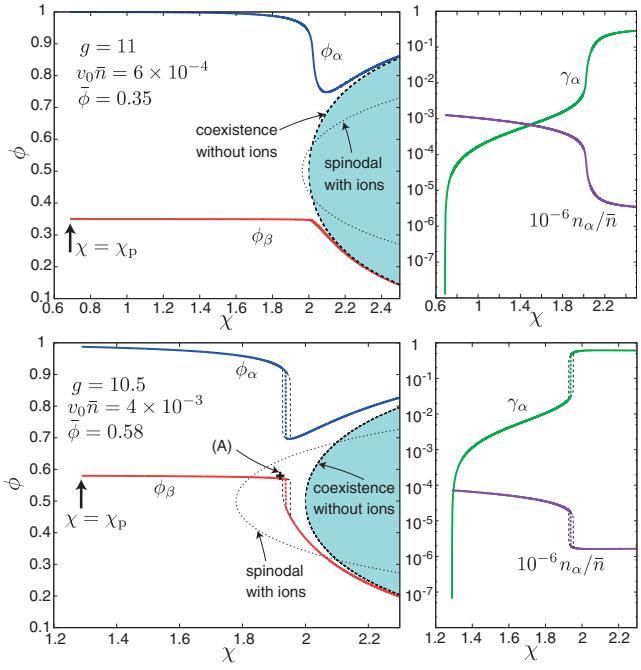

Figure 9. Left: compositions ϕ_α and ϕ_β vs. χ. Right: semilogarithmic plots of volume fraction γ_α and normalized solute density $n_\alpha/\bar{n}$ of the water-rich phase α vs. χ. Here $g = 11$, $\bar{\phi} = 0.35$, and $\bar{n} = 6 \times 10^{-4} v_0^{-1}$ (top), while $g = 10.5$, $\bar{\phi} = 0.58$, and $\bar{n} = 4 \times 10^{-3} v_0^{-1}$ (bottom). Plotted in the left also are the coexisting region without solute (in right green) and the spinodal curve with solute (on which the left hand side of eq 5.5 vanishes). See Figure 11 for simulation of phase separation on point (A) in the left bottom panel (Upper plates are from: R. Okamoto, A. Onuki, *Phys. Rev. E: Stat., Nonlinear, Soft Matter Phys.* **2010**, *82*, 051501).

where $A_1 = k_B T \bar{n}[\ln(\bar{n}\lambda^3) - 1]$ is a constant at fixed $\bar{n}$. In terms of ϕ_α, ϕ_β, and γ_α, eq 5.8 is rewritten as

$$\langle f_{\rm tot}\rangle = [\gamma_\alpha f(\phi_\alpha) + (1-\gamma_\alpha) f(\phi_\beta)] - k_B T \bar{n} \ln[\gamma_\alpha e^{g\phi_\alpha} + (1-\gamma_\alpha) e^{g\phi_\beta}] + A_1 \quad (5.9)$$

The second term ($\propto \bar{n}$) is relevant for large g (even for small $\bar{n}$). Now we should minimize $\langle f_{\rm tot}\rangle - h[\gamma_\alpha\phi_\alpha + (1-\gamma_\alpha)\phi_\beta - \bar{\phi}]$ with respect to ϕ_α, ϕ_β, and γ_α at fixed $\bar{\phi}$, where h appears as the Lagrange multiplier. Then we obtain the equilibrium conditions of two-phase coexistence,

$$h = f'(\phi_\alpha) - k_B T g n_\alpha = f'(\phi_\beta) - k_B T g n_\beta \quad (5.10)$$

$$f(\phi_\alpha) - f(\phi_\beta) - k_B T \Delta n = h \Delta\phi \quad (5.11)$$

These static relations hold even for ion pairs under eq 5.2.

5.3 Numerical Results of Two Phase Coexistence. In Figure 9, we give numerical results on the phase behavior of ϕ_α and ϕ_β in the left and n_α and γ_α in the right as functions of χ. We set $g = 11$, $\bar{\phi} = 0.35$, and $\bar{n} = 6 \times 10^{-4} v_0^{-1}$ in the top plates and $g = 10.5$, $\bar{\phi} = 0.58$, and $\bar{n} = 4 \times 10^{-3} v_0^{-1}$ in the bottom plates. The solute density is much larger in the latter case. Remarkably, a precipitation branch appears in the range,

$$\chi_{\rm p} < \chi < 2 \quad (5.12)$$

The volume fraction γ_α decreases to zero as χ approaches the lower bound $\chi_{\rm p} = \chi_{\rm p}(\bar{\phi}, \bar{n})$. Without solute, the mixture would be in one-phase states for $\chi < 2$. The precipitated domains are solute-rich with $\phi_\alpha \cong 1$, while ϕ_β is slightly larger than $\bar{\phi}$. In the left upper plate ϕ_α increases continuously with decreasing χ, while in the left lower plate ϕ_α jumps at $\chi = 1.937$ and hysteresis appears in the region $1.927 < \chi < 1.952$. We also plot the spinodal curve, $f''(\bar{\phi}) - k_B T g^2 \bar{n} = 0$, following from eq 5.5. Outside this curve, homogeneous states are metastable and precipitation can proceed via homogeneous nucleation in the bulk or via heterogeneous nucleation on hydrophilic surfaces of boundary plates or colloids.[32] Inside this curve, the system is linearly unstable and precipitation occurs via spinodal decomposition. This unstable region is expanded for $\bar{n} = 4 \times 10^{-3} v_0^{-1}$ in the lower plate.

5.4 Theory of Asymptotic Behavior for Large *g*. We present a theory of the precipitation branch in the limit $g \gg 1$ to determine $\chi_{\rm p}$ and $n_{\rm p}$. Assuming the branch (eq 5.12) at the starting point, we confirm its existence self-consistently.

We first neglect the term $-k_B T g n_\beta$ in eq 5.10 from $g v_0 n_\beta \ll 1$ and the term $f(\phi_\alpha)$ in eq 5.11 from $\phi_\alpha \cong 1$. In fact $g v_0 n_\beta \ll 1$ in Figure 9. We then obtain

$$h \cong f'(\phi_\beta) \cong -[f(\phi_\beta) + k_B T n_\alpha]/(1-\phi_\beta) \quad (5.13)$$

This determines the solute density n_α in phase α as a function of ϕ_β in the form,

$$n_\alpha \cong G(\phi_\beta)/k_B T \quad (5.14)$$

where $G(\phi)$ is a function of ϕ defined as

$$G(\phi) = -f(\phi) - (1-\phi) f'(\phi) = -(k_B T/v_0)[\ln\phi + \chi(1-\phi)^2] \quad (5.15)$$

From $dG/d\phi = -(1-\phi) f''(\phi) < 0$ and $G(1) = 0$, we have $G(\phi) > 0$ outside the coexistence curve, ensuring $n_\alpha > 0$ in eq 5.14.

In eq 5.10, we next use eq 3.3 for $f'(\phi_\alpha)$ to obtain

$$v_0^{-1} k_B T[-\ln(1-\phi_\alpha) - \chi - g v_0 n_\alpha] \cong f'(\phi_\beta) \quad (5.16)$$

where the logarithmic term ($\propto \ln(1-\phi)$) balances with the solvation term ($\propto g n_\alpha$). Use of eq 5.15 gives

$$1 - \phi_\alpha \cong A_\beta \exp[-g v_0 G(\phi_\beta)/k_B T] \quad (5.17)$$

where the coefficient A_β is given by

$$A_\beta = \exp[-\chi - v_0 f'(\phi_\beta)/k_B T] \quad (5.18)$$

so A_β is of order unity. The factor $\exp[-g v_0 G(\phi_\beta)/k_B T]$ in eq 5.17 is very small for $g \gg 1$, leading to $\phi_\alpha \cong 1$.

Furthermore, from eqs 5.6 and 5.7, the volume fraction γ_α of phase α is approximated as

$$\gamma_\alpha \cong \bar{n}/n_\alpha - e^{-g\Delta\phi} \cong k_B T \bar{n}/G(\phi_\beta) - e^{-g\Delta\phi} \quad (5.19)$$

The above relation is rewritten as

$$G(\phi_\beta) \cong k_B T \bar{n}/(\gamma_\alpha + e^{-g\Delta\phi}) \cong \frac{k_B T \bar{n}(1-\phi_\beta)}{\bar{\phi} - \phi_\beta + (1-\phi_\beta)\exp[-g(1-\phi_\beta)]} \quad (5.20)$$

From the first to second line, we have used eq 5.7 and replaced $\Delta\phi$ by $1 - \phi_\beta$. This equation determines ϕ_β and $\gamma_\alpha \cong$

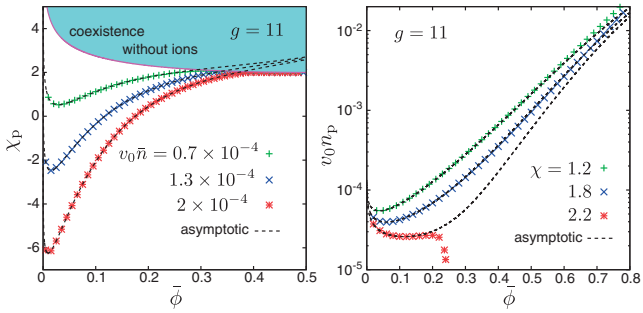

Figure 10. Left: $\chi_p(\bar{\phi}, \bar{n})$ vs. $\bar{\phi}$ for three values of $\bar{n}$ at $g = 11$, which nearly coincide with the asymptotic formula (eq 5.22) (dotted line) for $\bar{\phi} < 0.35$ and converge to the coexistence curve for larger $\bar{\phi}$. Coexistence region without ions is in the upper region (in right green). Right: $v_0 n_p(\bar{\phi}, \chi)$ vs. $\bar{\phi}$ on a semilogarithmic scale at $g = 11$, It coincides with the asymptotic formula (eq 5.23) (dotted line) for $\chi < 2$ and tends to zero at the coexistence composition, 0.249 (top) or 0.204 (bottom) (From: R. Okamoto, A. Onuki, *Phys. Rev. E: Stat., Nonlinear, Soft Matter Phys.* **2010**, *82*, 051501).

$(\bar{\phi} - \phi_\beta)/(1 - \phi_\beta)$. We recognize that $G(\phi_\beta)$ increases up to $T\bar{n}e^{g\Delta\phi} \cong T\bar{n}e^{g(1-\bar{\phi})}$ as $\gamma_\alpha \to 0$ or as $\phi_\beta \to \bar{\phi}$. In this limit it follows the marginal relation,

$$G(\bar{\phi}) \cong k_B T \bar{n} e^{g(1-\bar{\phi})} \quad (\gamma_\alpha \to 0) \tag{5.21}$$

If $\bar{n}$ is fixed, this relation holds at $\chi = \chi_p$ so that

$$\chi_p \cong [-\ln\bar{\phi} - v_0\bar{n}e^{g(1-\bar{\phi})}]/(1-\bar{\phi})^2 \tag{5.22}$$

where we use the second line of eq 5.15. Here $\bar{n}$ appears in the combination $\bar{n}e^{g(1-\bar{\phi})}(\gg \bar{n})$. On the other hand, if χ is fixed, eq 5.21 holds at $\bar{n} = n_p$. Thus the minimum solute density n_p is estimated as

$$n_p \cong e^{-g(1-\bar{\phi})} G(\bar{\phi})/k_B T \tag{5.23}$$

which is much decreased by the small factor $e^{-g(1-\bar{\phi})}$.

In Figure 10, the curves of χ_p and n_p nearly coincide with the asymptotic formulas (eqs 5.22 and 5.23) in the range $\bar{\phi} < 0.35$ for χ_p and in the range $\chi < 2$ for n_p. They exhibit a minimum at $\bar{\phi} \approx e^{-g}/v_0\bar{n}g$ for χ_p and at $\bar{\phi} \approx g^{-1}$ for n_p. For larger $\bar{\phi} > 0.35$, χ_p nearly coincide with the coexistence curve, indicating disappearance of the precipitation branch. Notice that n_p decreases to zero as $\bar{\phi}$ approaches the coexistence composition $\phi_{cx} = 0.249$ at $\chi = 2.2$ (top) and 0.204 at $\chi = 2.3$ (bottom), where phase separation occurs without solute.

5.5 Simulation of Spinodal Decomposition for Hydrophilic Ions. In our theory[32] we investigated solute-induced nucleation starting with homogeneous metastable states outside the spinodal curve (dotted line) in the left panels of Figure 9. Here, we show two-dimensional numerical results of spinodal decomposition for hydrophilic ions with $g_1 = 12$, $g_2 = 9$, $e^2/\varepsilon_0 k_B T = 3a$, and $\varepsilon_1 = \varepsilon_0$. At $t = 0$, we started with point (A) inside the spinodal curve in the left lower panel in Figure 9 using the common values of the static parameters given by $\chi = 1.92$, $\bar{\phi} = 0.58$, and $\bar{n} = \langle n_1 + n_2\rangle = 4 \times 10^{-3}/v_0$. In addition, we set $C = 2k_B T a^2/v_0$. On a 256×256 lattice under the periodic boundary condition, we integrated eq 3.36 for the composition $\phi(\boldsymbol{r}, t)$ with the velocity field $\boldsymbol{v}(\boldsymbol{r}, t)$ being

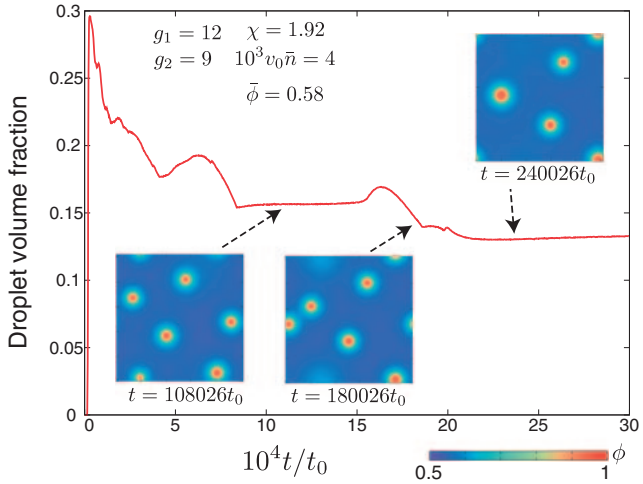

Figure 11. Time evolution of droplet volume fraction (that of the region $\phi > 0.6$) and composition snapshots of precipitated droplets at three times. They are induced by hydrophilic ions with $g_1 = 12$ and $g_1 = 9$. The initial state was at point (A) in Figure 9 with $\chi = 1.92$, $\bar{\phi} = 0.58$, and $\bar{n} = 4 \times 10^{-3} v_0^{-1}$. The droplet volume fraction nearly tends to a constant.

determined by the Stokes approximation in eq 3.37. The cations and anions obey

$$\frac{\partial n_i}{\partial t} + \nabla \cdot (n_i \boldsymbol{v}) = \frac{D}{k_B T} \nabla \cdot n \nabla \mu_i$$
$$= D\nabla \cdot [\nabla n_i - g_i n_i \nabla\phi - Z_i e n_i \boldsymbol{E}] \tag{5.24}$$

where $i = 1, 2$. The chemical potentials μ_i are defined in eq 3.11 and the ion diffusion constants are commonly given by D. The space mesh size is $a = v_0^{1/d}$ with $d = 2$. We measure time in units of $t_0 = a^2 v_0/L_0$ and set $D = a^2/t_0$ and $\eta_0 = 0.15 k_B T t_0/v_0$, where L_0 is the kinetic coefficient for the composition and η_0 is the shear viscosity.

In Figure 11, we show the time evolution of the droplet volume fraction, which is the fraction of the region $\phi > 0.6$. In the early stage, the droplet number decreases in time with the evaporation and condensation mechanism. In the late stage, it changes very slowly tending to a constant. In our simulation without random noise, the droplets do not undergo Brownian motion and the droplet collision is suppressed. We also performed a simulation for a neutral solute with $g = 10.5$ (not shown here), which exhibits almost the same phase separation behavior as in Figure 11.

6. Theory of Polyelectrolytes

6.1 Weakly Ionized Polyelectrolytes. In this section, we consider weakly charged polymers in a theta or poor, one-component water-like solvent in the semidilute case $\phi > N^{-1/2}$. Following the literature of polymer physics,[5] we use ϕ and N to represent the polymer volume fraction and the polymerization index. Here charged particles interact differently between uncharged monomers and solvent molecules. The selective solvation should become more complicated for mixture solvents, as discuused in Section **1**.

To ensure flexibility of the chains, we assume that the fraction of charged monomers on the chains, denoted by f_{ion}, is

small or $f_{\rm ion} \ll 1$. From the scaling theory,[5] the polymers consist of blobs with monomer number $g_{\rm b} = \phi^{-2}$ with length $\xi_{\rm b} = a g_b^{1/2} = a\phi^{-1}$. The electrostatic energy within a blob is estimated as

$$\epsilon_{\rm b} = k_{\rm B}T(f_{\rm ion}g)^2\ell_{\rm B}/\xi_{\rm b} = k_{\rm B}T f_{\rm ion}{}^2\ell_{\rm B}/\phi^3\alpha \tag{6.1}$$

where $\ell_{\rm B}$ is the Bjerrum length. The blobs are not much deformed under the weak charge condition $\epsilon_{\rm b} < k_{\rm B}T$, which is rewritten as

$$\phi > f_{\rm ion}{}^{2/3}(\ell_{\rm B}/a)^{1/3} \tag{6.2}$$

6.2 Ginzburg–Landau Theory. The number of the ionizable monomers (with charge $-e$) on a chain is written as $\nu_{\rm M}N$ with $\nu_{\rm M} < 1$. Then the degree of ionization (or dissociation) is $\zeta = f_{\rm ion}/\nu_{\rm M}$ and the number density of the ionized monomers is

$$n_{\rm p} = v_0{}^{-1} f_{\rm ion}\phi = v_0{}^{-1}\nu_{\rm M}\zeta\phi \tag{6.3}$$

The charge density is expressed as

$$\rho = e\sum_{i=c,1,2} Z_i n_i - e n_{\rm p} \tag{6.4}$$

Here $i = c$ represents the counter ions, $i = 1$ the added cations, and $i = 2$ the added anions. The required relation $f_{\rm ion} \ll 1$ becomes $\nu_{\rm M}\zeta \ll 1$ (which is satisfied for any ζ if $\nu_{\rm M} \ll 1$).

We set up the free energy F accounting for the molecular interactions and the ionization equilibrium.[33] Then F assumes the standard form (eq 3.1), where the coefficient of the gradient free energy is written as[5,36]

$$C(\phi) = k_{\rm B}T/12a\phi(1-\phi) \tag{6.5}$$

in terms of the molecular length $a = v_0{}^{1/3}$ and ϕ. The $f_{\rm tot}$ consists of four parts as

$$f_{\rm tot} = f(\phi) + k_{\rm B}T\sum_{i=c,1,2} n_i[\ln(n_i\lambda_i{}^3) - 1 + g_i\phi] + k_{\rm B}T(\Delta_0 + g_{\rm p}\phi)n_{\rm p} + f_{\rm dis} \tag{6.6}$$

The first term f is of the Flory–Huggins form,[5,36]

$$\frac{v_0 f}{k_{\rm B}T} = \frac{\phi}{N}\ln\phi + (1-\phi)\ln(1-\phi) + \chi\phi(1-\phi) \tag{6.7}$$

The coupling terms ($\propto g_i g_{\rm p}$) arise from the molecular interactions among the charged particles (the ions and the charged monomers) and the uncharged particles (the solvent particles and the uncharged monomers), while $k_{\rm B}T\Delta_0$ is the dissociation free energy in the dilute limit of polymers ($\phi \to 0$). The last term in $f_{\rm tot}$ arises from the dissociation entropy on chains,[60–62]

$$\frac{v_0}{k_{\rm B}T} f_{\rm dis} = \nu_{\rm M}\phi[\zeta\ln\zeta + (1-\zeta)\ln(1-\zeta)] \tag{6.8}$$

6.3 Dissociation Equilibrium. If F is minimized with respect to ζ, it follows the equation of ionization equilibrium or the mass action law,

$$n_{\rm c}\zeta/(1-\zeta) = K(\phi) \tag{6.9}$$

where $n_{\rm c}$ is the counter ion density and $K(\phi)$ is the dissociation constant of the form,

$$K(\phi) = v_0{}^{-1}\exp[-\Delta_0 - (g_{\rm p} + g_{\rm c})\phi] \tag{6.10}$$

We may interpret $k_{\rm B}T[\Delta_0 + (g_{\rm p} + g_{\rm c})\phi]$ as the composition-dependent dissociation free energy. With increasing the polymer volume fraction ϕ, the dissociation decreases for positive $g_{\rm p} + g_{\rm c}$ and increases for negative $g_{\rm p} + g_{\rm c}$. If $g_{\rm p} + g_{\rm c} \gg 1$, $K(\phi)$ much decreases even for a small increase of ϕ. Here $K(\phi)$ has the meaning of the crossover counter ion density since ζ is expressed as

$$\zeta = 1/[1 + n_{\rm c}/K(\phi)] \tag{6.11}$$

which decreases appreciably for $n_{\rm c} > K(\phi)$.

In particular, if there is no charge density and no salt ($n_{\rm p} = n_{\rm c}$ and $n_1 = n_2 = 0$), $n_{\rm c}$ satisfies the quadratic equation $n_{\rm c}(n_{\rm c} + K) = v_0^{-1}\nu_{\rm M}\phi K$, which is solved to give

$$\zeta = v_0 n_{\rm c}/\nu_{\rm M}\phi = 2/(\sqrt{Q(\phi)+1} + 1) \tag{6.12}$$

Here it is convenient to introduce

$$Q(\phi) = 4\nu_{\rm M}\phi/v_0 K(\phi) \tag{6.13}$$

We find $\zeta \ll 1$ and $n_{\rm c} \cong (\nu_{\rm M}\phi K/v_0)^{1/2}$ for $Q \gg 1$, while $\zeta \to 1$ for $Q \ll 1$. The relation (eq 6.12) holds approximately for small charge densities without salt.

6.4 Structure Factor. As in Section **3**, it is straightforward to calculate the structure factor $S(q)$ for the fluctuations of ϕ on the basis of $f_{\rm tot}$ in eq 6.6. As a function of the wavenumber q, it takes the same functional form as in eq 3.14, while the coefficients in the polyelectrolyte case are much more complicated than those in the electrolyte case. That is, the shift $-(g_1 + g_2)^2 n_0/2$ in eq 3.14 is replaced by its counterpart Δr dependent on n_i and $n_{\rm p}$ (for which see our paper[33]). In the following expressions (eqs 6.14–6.17), n_i, $n_{\rm p}$, and ϕ represent the average quantities. The Debye wavenumber of polyelectrolytes is given by[60]

$$\kappa^2 = 4\pi\ell_{\rm B}\left[(1-\zeta)n_{\rm p} + \sum_i Z_i^2 n_i\right] \tag{6.14}$$

which contains the contribution from the (monovalent) ionized monomers ($\propto n_{\rm p}$). The asymmetry parameter $\gamma_{\rm p}$ in eq 3.14 is of the form,

$$\gamma_{\rm p} = (4\pi\ell_{\rm B}k_{\rm B}T/C)^{1/2}A/\kappa^2 \tag{6.15}$$

where C is given by eq 6.5 and

$$A = n_{\rm p}/\phi - (1-\zeta)g_{\rm p}n_{\rm p} + \sum_i Z_i g_i n_i \tag{6.16}$$

In this definition, $\gamma_{\rm p}$ can be negative depending on the terms in A. Mesophase formation can appear for $|\gamma_{\rm p}| > 1$ with increasing χ.

The parameter $\gamma_{\rm p}$ is determined by the ratios among the charge densities and is nonvanishing even in the dilute limit of the charge densities. In particular, if $n_{\rm c} = n_{\rm p}$ and $n_1 = n_2$ in the monovalent case, $\gamma_{\rm p}$ is simplified as

$$\gamma_{\rm p} = \frac{\phi^{-1} - (1-\zeta)g_{\rm p} + g_{\rm c} + (g_1 - g_2)R}{(4\pi\ell_{\rm B}C/k_{\rm B}T)^{1/2}(2 - \zeta + 2R)} \tag{6.17}$$

where the counter ions and the added cations are different. The $R \equiv n_1/n_{\rm p}$ is the ratio between the salt density and the that of ionized monomers and eq 6.5 gives $(4\pi\ell_{\rm B}C/k_{\rm B}T)^{1/2} = [\pi\ell_{\rm B}/3a\phi(1-\phi)]^{1/2}$.

Some consequences follow from eq 6.17. (i) With enriching a salt we eventually have $R \gg |g_i|$; then, the above formula tends to eq 3.15, which is applicable for neutral polymer solutions (and low-molecular-weight binary mixtures for $N = 1$) with salt. (ii) Without the solvation or for $g_i = 0$, the above $S(q)$ tends to the previous expressions for polyelectrolytes,[60,93,94] where γ_p decreases with increasing R. In accord with this, Braun et al.[95] observed a mesophase at low salt contents and macrophase separation at high salt contents. (iii) In our theory, neutral polymers in a polar solvent can exhibit a mesophase for large $|g_1 - g_2|$.

Hakem et al.[96,97] found a broad peak at an intermediate wavenumber in the scattering amplitude in (neutral) polyethylene-oxide (PEO) in methanol and in acetonitrile by adding a small amount of salt KI. They ascribed the origin of the peak to binding of K^+ to PEO chains. Here more experiments are informative. An experiment by Sadakane et al.[39] suggests that use of an antagonistic salt would yield mesophases more easily.

6.5 Interface Profiles without Salt. We suppose coexistence of two salt-free phases ($n_1 = n_2 = 0$), separated by a planar interface. Even without salt, the interface profiles are extremely varied, sensitively depending on the molecular interaction parameters, Δ_0, g_p, and g_c. If a salt is added, they furthermore depend on g_1, g_2, and the salt amount. The quantities with the subscript α (β) denote the bulk values in the polymer-rich (solvent-rich) phase attained as $z \to -\infty$ (as $z \to \infty$). The ratio of the bulk counter ion densities is given by

$$\frac{n_{c\alpha}}{n_{c\beta}} = \frac{\phi_\alpha \zeta_\alpha}{\phi_\beta \zeta_\beta} = \exp\left[-g_c \Delta\phi - \frac{e\Delta\Phi}{k_B T}\right] \tag{6.18}$$

The Galvani potential difference $\Delta\Phi = \Phi_\alpha - \Phi_\beta$ is expressed in terms of $Q(\phi)$ in eq 6.13 as

$$\frac{e\Delta\Phi}{k_B T} = g_p \Delta\phi + \ln\left[\frac{\sqrt{Q(\phi_\beta)+1}-1}{\sqrt{Q(\phi_\alpha)+1}-1}\right] \tag{6.19}$$

If $Q(\phi_\alpha) \gg 1$ and $Q(\phi_\beta) \gg 1$ (or $\zeta_\alpha \ll 1$ and $\zeta_\beta \ll 1$), we obtain $e\Delta\Phi/k_B T \cong (g_p - g_c)\Delta\phi/2 + \ln(\phi_\beta/\phi_\alpha)$.

We give numerical results of one-dimensional profiles in equilibrium, where we set $\chi = 1$, $N = 20$, $\varepsilon_1 = -0.9\varepsilon_0$, and $\ell_B = e^2/\varepsilon_0 T = 8a/\pi$. The dielectric constant of the solvent is 10 times larger than that of the polymer. The space will be measured in units of the molecular size $a = v_0^{1/3}$. In Figure 12, we show salt-free interface profiles for (a) $\Delta_0 = 5$, $g_p = 1$, and $g_c = 4$ and (b) $\Delta_0 = 8$, $g_p = 2$, and $g_c = -6$. In the α and β regions, the degree of ionization ζ is 0.071 and 0.65 in (a) and is 0.24 and 0.51 in (b), respectively. The normalized potential drop $e(\Phi_\alpha - \Phi_\beta)/k_B T$ is -2.67 in (a) and 0.099 in (b). Interestingly, in (b), $\Phi(z)$ exhibits a deep minimum at the interface position. We can see appearance of the charge density $n_c - n_p$ around the interface, resulting in an electric double layer. The counter ion density is shifted to the β region in (a) because of positive g_c and to the α region in (b) because of negative g_c. The parameter γ_p in eq 6.16 is 0.75 in (a) and 0.20 in (b) in the α region, ensuring the stability of the α region.

The surface tension σ is again expressed as in eq 3.26 with the negative electrostatic contribution. It is calculated as $\sigma = 0.0175 k_B T/a^2$ in (a) and as $0.0556 k_B T/a^2$ in (b), while we obtain $\sigma = 0.050 k_B T/a^2$ without ions at the same $\chi = 1$. In

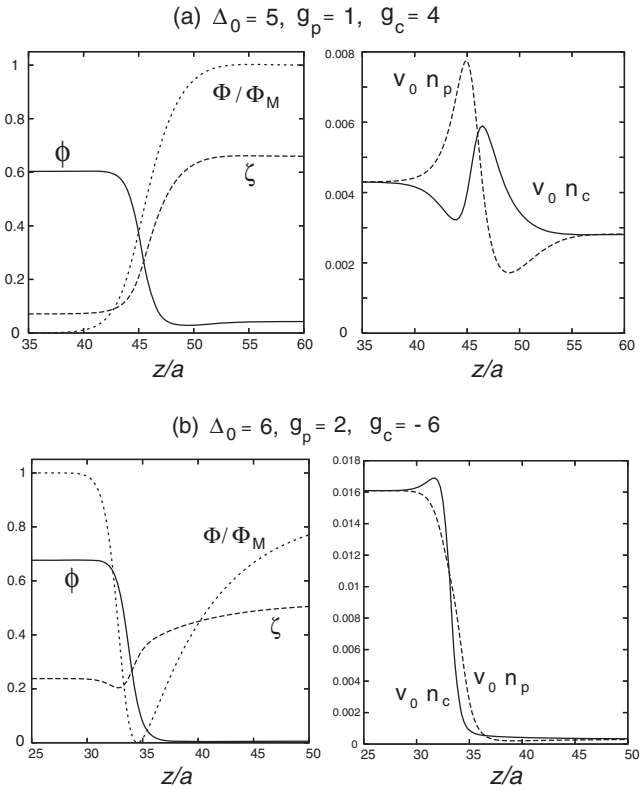

Figure 12. Interface profiles in the salt-free case for (a) $\Delta_0 = 5$, $g_p = 1$, and $g_c = 4$ (top) and for (b) $\Delta_0 = 8$, $g_p = 2$, and $g_c = -6$ (bottom). Polymer volume fraction $\phi(z)$, normalized potential $\Phi(z)/\Phi_M$, and degree of ionization $\zeta(z)$ (left), and normalized charge densities $v_0 n_c(z)$ and $v_0 n_p(z)$ (right). The other parameters are common as $\chi = 1$, $N = 20$, $\nu_M = 0.1$, $\varepsilon_1 = -0.9\varepsilon_0$, and $\ell_B = 8a/\pi$. Here $\Phi(z)$ is measured from its minimum, and Φ_M ($=2.67 k_B T/e$ in (a) and $6.86 k_B T/e$ in (b)) is the difference of its maximum and minimum (From: A. Onuki, R. Okamoto, *J. Phys. Chem. B* **2009**, *113*, 3988).

(a) σ is largely decreased because the electrostatic term σ_e in eq 3.27 is increased due to the formation of a large electric double layer. In (b), on the contrary, it is increased by 10% due to depletion of the charged particles from the interface.[23]

We mention calculations of the interface profiles in weakly charged polyelectrolytes in a poor solvent using self-consistent field theory.[98,99] In these papers, however, the solvation interaction was neglected.

6.6 Periodic States without Salt. With varying the temperature (or χ), the average composition $\langle\phi\rangle$, the amount of salt, there can emerge a number of mesophases sensitively depending on the various molecular parameters (g_i, Δ_0, and ν_M). In Figure 13, we show an example of a one-dimensional periodic state without salt. Here ν_M is set equal to 0.5 and the charge densities are much increased. In this case, the degree of segregation and the charge heterogeneities are much milder than in the cases in Figure 12.

7. Summary and Remarks

In this review, we have tried to demonstrate the crucial role of the selective solvation of a solute in phase transitions of

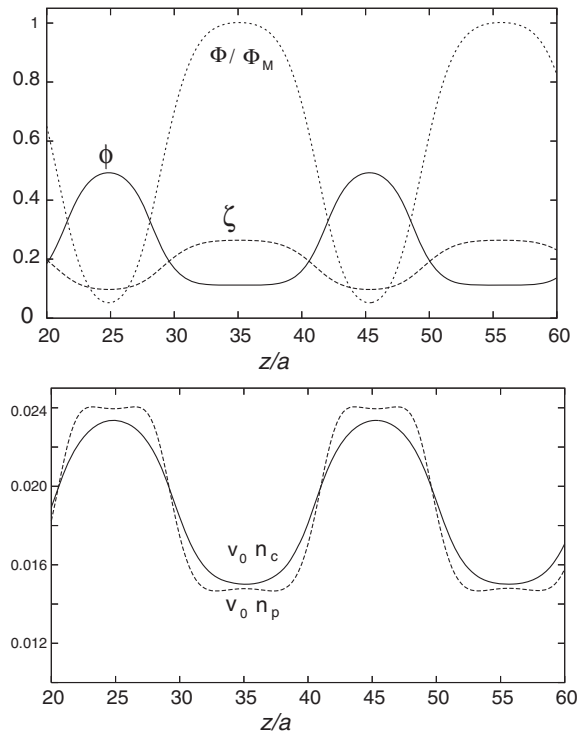

Figure 13. Periodic profiles in a salt-free mesophase with $\nu_M = 0.5$, $\Delta_0 = 5$, $g_p = 1$, and $g_c = 4$. Top: $\phi(z)$. $\Phi(z)/\Phi_M$ with $\Phi_M = 0.86T/e$, and $\zeta(z)$. Bottom: $v_0 n_c(z)$ and $v_0 n_p(z)$ (From: A. Onuki, R. Okamoto, *J. Phys. Chem. B* **2009**, *113*, 3988).

various soft materials. We have used coarse-grained approaches to investigate mesoscopic solvation effects. Selective solvation should be relevant in understanding a wide range of mysterious phenomena in water. Particularly remarkable in polar binary mixtures are mesophase formation induced by an antagonistic salt and precipitation induced by a one-sided solute (a salt composed of hydrophilic cations and anions and a neutral hydrophobic solute). Regarding the first problem, our theory is still insufficient and cannot well explain the complicated phase behavior disclosed by the experiments.[39–41] To treat the second problem, we have started with the free energy density f_{tot} in eq 5.1, which looks rather obvious but yields highly nontrivial results for large g. Systematic experiments are now possible. In particular, this precipitation takes place on colloid surfaces as a prewetting phase transition near the precipitation curve $\chi = \chi_p$ as in Figure 10.[32]

Though still preliminary, we have also treated an ionic surfactant system, where added in water–oil are cationic surfactant, anionic counter ions, and ions from a salt. In this case, we have introduced the amphiphilic interaction as well as the solvation interaction to study the interface adsorption. For ionic surfactants, the Gibbs formula[6,89] for the surface tension is insufficient, because it neglects the electrostatic interaction.

In polyelectrolytes, the charge distributions are extremely complex around interfaces and in mesophases, sensitively depending on the molecular interaction and the dissociation process. Our continuum theory takes into account these effects in the simplest manner, though our results are still fragmentary. Salt effects in polyelectrolytes should also be further studied, on which some discussions can be found in our previous paper.[33] In the future, we should examine phase separation processes in polyelectrolytes, where the composition, the ion densities, and the degree of ionization are highly inhomogeneous. In experiments, large-scale heterogeneities have been observed to be pinned in space and time,[100,101] giving rise to enhanced scattering at small wavenumbers.

As discussed in Section **1**, there can be phase separation induced by selective hydrogen bonding. In particular, the effect of moisture uptake is dramatic in PS–PVME,[58] where scattering experiments controlling the water content are desirable. To investigate such polymer blends theoretically, we may use the form in eq 5.1 with n being the water density and $f(\phi)$ being the Flory–Huggins free energy for polymer blends.[5] Similar problems should also be encountered in block polymer systems containing ions or water. It is also known that blends of block polymer and homopolymer exhibit complicated phase behavior for different interaction parameters χ_{ij}.[102]

We mention two interesting effects not discussed in this review. First, there can be an intriguing interplay between the solvation and the hydrogen bonding in phase separation. For example, in some aqueous mixtures, even if they are miscible at all T at atmosphere pressure without salt, addition of a small amount of a hydrophilic salt gives rise to reentrant phase separation behavior.[13–16] On the other hand, Sadakane et al. observed a shrinkage of a closed-loop coexistence curve by adding an atagonistic salt or an ionic surfactant.[40] Second, molecular polarization of polar molecules or ions can give rise to a surface potential difference on the molecular scale at an interface. See such an example for water–hexane.[103] This effect is particularly noteworthy for hydronium ions in acid solutions.[88]

We will report on the wetting transition on charged walls, rods, and colloids and the solvation-induced colloid interaction. These effects are much influenced by the ion-induced precipitation discussed in Section **5**. In these problems, first-order prewetting transitions occur from weak-to-strong ionization and adsorption, as discussed in our paper on charged rods.[34] We will also report that a small amount of a hydrophobic solute can produce small bubbles in water even outside the coexistence curve, on which there have been a large number of experiments.

Appendix

A: Statistical Theory of Selective Solvation at Small Water Composition. We present a simple statistical theory of binding of polar molecules to hydrophilic ions due to the ion–dipole interaction in a water–oil mixture[34] when the water volume fraction ϕ is small. We assume no macroscopic inhomogeneity and do not treat the large-scale electrostatic interaction. Similar arguments were given for hydrogen boning between water and polymer.[54,55]

Our system has a volume V and contains N_w water molecules. Using the water molecular volume v_0, we have

$$\phi = N_w v_0/V = N_w/N_0 \tag{A1}$$

where $N_0 = V/v_0$. We fix N_w or ϕ in the following. The total ion numbers are denoted by $N_{Ii} = Vn_i$, where $i = 1$ for the cations and $i = 2$ for the anions with n_i being the average densities. The ionic volumes are assumed to be small and their

volume fractions are neglected. Then the oil volume fraction is given by $1-\phi$. Each solvation shell consists of ν water molecules with $\nu = 1, \ldots, Z_i$, where Z_i is the maximum water number in a shell.

Let the number of the ν-clusters composed of ν water molecules around an ion be $\gamma_{i\nu}N_{\rm w}$. The total number of the solvated ions is then $\gamma_i N_{\rm Ii}$ with

$$\gamma_i = \sum_\nu \gamma_{i\nu} < 1 \tag{A2}$$

where $1 \le \nu \le Z_i$. The number of the bound water molecules in the ν-clusters is $\nu\gamma_{i\nu}N_{\rm Ii}$. The fraction of the unbound water molecules $\phi_{\rm f}$ satisfies

$$\phi_{\rm f} + v_0 n_i \sum_{i,\nu} \nu\gamma_{i\nu} = \phi \tag{A3}$$

We construct the free energy of the total system $F_{\rm tot}$ for each given set of $\gamma_{i\nu}$. In terms of the oil density $n_{\rm oil} = {v_0}^{-1}(1-\phi)$, the unbound water density $n_{\rm wf} = {v_0}^{-1}\phi_{\rm f}$, the unbound ion densities $n_{i\rm f} = n_i(1-\gamma_i)$, and the cluster densities $n_{i\nu} = n_i\gamma_{i\nu}$, we obtain

$$\begin{aligned}\frac{F_{\rm tot}}{Vk_{\rm B}T} &= n_{\rm oil}[\ln(n_{\rm oil}{\lambda_{\rm oil}}^3) - 1] + n_{\rm wf}[\ln(n_{\rm wf}{\lambda_{\rm w}}^3) - 1] \\ &\quad + \sum_i [n_{i\rm f}\ln(n_{i\rm f}{\lambda_i}^3) - n_i] + \sum_{i,\nu} n_{i\nu}[\ln(n_{i\nu}{\lambda_{i\nu}}^3) - w_{i\nu}^0] \\ &\quad + \chi v_0 n_{\rm oil} n_{\rm wf} + \sum_{i,\nu} \chi_{i\nu} v_0 n_{i\nu} n_{\rm oil}\end{aligned} \tag{A4}$$

where $\lambda_{\rm oil}$, $\lambda_{\rm w}$, λ_i, and $\lambda_{i\nu}$ are the thermal de Broglie wavelengths, $k_{\rm B}Tw_{i\nu}^0$ are the "bare" binding free energies, and χ is the interaction parameter between the unbound water and the oil. We asssume short-range interactions among the clusters and the oil characterized by the interaction parameters $\chi_{i\nu}$ to obtain the last term. At small ϕ, the interactions among the clusters and the unbound water are neglected. That is, we neglect the contributions of order ϕ^2. We then calculate the solvation contribution $F_{\rm sol} \equiv F_{\rm tot} - F_0$, where F_0 is the free energy without binding ($\gamma_{i\nu} = 0$). Some calculations give

$$\begin{aligned}\frac{F_{\rm sol}}{N_0 k_{\rm B}T} &= \phi_{\rm f}(\ln\phi_{\rm f} - 1) + \sum_i n_i(1-\gamma_i)\ln(1-\gamma_i) \\ &\quad + \sum_{i,\nu} n_i\gamma_{i\nu}(\ln\gamma_{i\nu} - w_{i\nu}) - \phi(\ln\phi - 1)\end{aligned} \tag{A5}$$

where $k_{\rm B}Tw_{i\nu}$ are the "renormalized" binding free energies written as

$$w_{i\nu} = w_{i\nu}^0 + 3\ln(\lambda_i{\lambda_{\rm w}}^\nu/\lambda_{i\nu}) + \nu\chi - \chi_{i\nu} \tag{A6}$$

The fractions $\gamma_{i\nu}$ are determined by minimization of $F_{\rm sol}$ with respect to $\gamma_{i\nu}$ under eqs A2 and A3 as

$$\gamma_{i\nu} = (1-\gamma_i){\phi_{\rm f}}^\nu e^{w_{i\nu}} \tag{A7}$$

$$\gamma_i = 1 - 1/\left(1 + \sum_\nu \phi_{\rm f}^\nu e^{w_{i\nu}}\right) \tag{A8}$$

Substitution of eqs A7 and A8 into eq A5 yields

$$\frac{F_{\rm sol}}{k_{\rm B}TN_0} = \phi\ln\frac{\phi_{\rm f}}{\phi} + \phi - \phi_{\rm f} + \sum_i v_0 n_i \ln(1-\gamma_i) \tag{A9}$$

First, we assume the dilute limit of ions $N_{\rm I} \ll N_{\rm w}$, where we have $\phi - \phi_{\rm f} \ll \phi$. In the right hand side of eq A9, the sum of the first three terms becomes $-(\phi-\phi_{\rm f})^2/2\phi$ and is negligible. We write $F_{\rm sol}$ as the sum $V\sum_i n_i\mu_{\rm sol}^i(\phi)$ and use eq A8 to obtain the solvation chemical potentials of the form,

$$\mu_{\rm sol}^i(\phi) = -k_{\rm B}T\ln\left(1 + \sum_\nu \phi^\nu e^{w_{i\nu}}\right) \tag{A10}$$

Let the maximum of $k_{\rm B}Tw_{i\nu}/\nu$ (per molecule for various ν) be $\epsilon_{{\rm b}i}$ for each i (eq 2.3). Then we obtain the expression (eq 2.2) for the crossover volume fraction $\phi_{\rm sol}^i$. For $\phi > \phi_{\rm sol}^i$, γ_i approaches unity.

Second, we consider the dilute limit of water, $\phi \ll \phi_{\rm sol}^i$ ($i = 1, 2$), where the cluster fractions ν_i are small and the dimers with $\nu = 1$ are dominant as indicated in the experiment.[69] Neglecting the contributions from the clusters with $\nu \ge 2$, we obtain

$$\gamma_i \cong \phi_{\rm f}e^{w_{i1}}, \quad \phi_{\rm f} \cong \phi/(1+S) \tag{A11}$$

where S is the parameter defined as

$$S = v_0(n_1e^{w_{11}} + n_2e^{w_{21}}) \tag{A12}$$

The solvation free energy behaves as

$$F_{\rm sol}/N_0k_{\rm B}T \cong -\phi\ln(1+S) \tag{A13}$$

For $S \ll 1$, we find $\mu_{\rm sol}^i(\phi) \cong -k_{\rm B}T\phi e^{w_{1i}}$. However, if $S \gtrsim 1$, the solvation chemical potential are not well defined.

B: Ions at Liquid–Liquid Interface. In electrochemistry, attention has been paid to the ion distribution and the electric potential difference across a liquid–liquid interface[74,75] (In the vicinity of an air–water interface, virtually no ions are present in the bulk air region.[80,81]). Let us suppose two species of ions ($i = 1, 2$) with charges Z_1e and Z_2e ($Z_1 > 0$, $Z_2 < 0$). At low ion densities, the total ion chemical potentials μ_i in a mixture solvent are expressed as

$$\mu_i = k_{\rm B}T\ln(n_i{\lambda_i}^3) + Z_ie\Phi + \mu_{\rm sol}^i(\phi) \tag{B1}$$

where λ_i is the thermal de Broglie length (but is an irrelevant constant in the isothermal condition) and Φ is the local electric potential. This quantity is a constant in equilibrium. For neutral hydrophobic particles the electrostatic term is nonexistent, so we have eq 2.5.

We consider a liquid–liquid interface between a polar (water-rich) phase α and a less polar (oil-rich) phase β with bulk compositions ϕ_α and ϕ_β with $\phi_\alpha > \phi_\beta$. The bulk ion densities far from the interface are written as $n_{i\alpha}$ in phase α and $n_{i\beta}$ in phase β. From the charge neutrality condition in the bulk regions, we require

$$Z_1n_{1\alpha} + Z_2n_{2\alpha} = 0, \quad Z_1n_{1\beta} + Z_2n_{2\beta} = 0 \tag{B2}$$

The potential Φ tends to constants Φ_α and Φ_β in the bulk two phases, yielding a Galvani potential difference, $\Delta\Phi = \Phi_\alpha - \Phi_\beta$. Here Φ approaches its limits on the scale of the Debye screening lengths, ${\kappa_\alpha}^{-1}$ and ${\kappa_\beta}^{-1}$, away from the interface, so we assume that the system extends longer than ${\kappa_\alpha}^{-1}$ in phase α and ${\kappa_\beta}^{-1}$ in phase β. Here we neglect molecular polarization of solvent molecules and surfactant molecules at an interface (see comments in the summary section).

The solvation chemical potentials $\mu^i_{\rm sol}(\phi)$ also take different values in the two phases due to their composition dependence. So we define the differences $\Delta\mu^i_{\alpha\beta}$ as in eq 2.4. The continuity of μ_i across the interface gives

$$k_{\rm B}T\ln(n_{i\alpha}/n_{i\beta}) + Z_i e\Delta\Phi - \Delta\mu^i_{\alpha\beta} = 0 \tag{B3}$$

where $i = 1, 2$. From eqs B2 and B3, the Galvani potential difference $\Delta\Phi$ is expressed as[23,75]

$$\Delta\Phi = [\Delta\mu^1_{\alpha\beta} - \Delta\mu^2_{\alpha\beta}]/e(Z_1 + |Z_2|) \tag{B4}$$

Similar potential differences also appear at liquid–solid interfaces (electrodes).[74] The ion densities in the bulk two phases (in the dilute limit) are simply related by

$$\frac{n_{1\beta}}{n_{1\alpha}} = \frac{n_{2\beta}}{n_{2\alpha}} = \exp\left[-\frac{|Z_2|\Delta\mu^1_{\alpha\beta} + Z_1\Delta\mu^2_{\alpha\beta}}{(Z_1 + |Z_2|)k_{\rm B}T}\right] \tag{B5}$$

However, if three ion species are present, the ion partitioning between two phases is much more complicated.[24]

This work was supported by KAKENHI (Grant-in-Aid for Scientific Research) on Priority Area Soft Matter Physics from the Ministry of Education, Culture, Sports, Science and Technology of Japan. Thanks are due to informative discussions with M. Anisimov, K. Sadakane, H. Seto, T. Kanaya, K. Nishida, T. Osakai, T. Hashimoto, and F. Tanaka.

References

1 Y. Levin, *Rep. Prog. Phys.* **2002**, *65*, 1577.
2 J.-L. Barrat, J.-F. Joanny, in *Advances in Chemical Physics: Polymeric Systems*, ed. by I. Prigogine, S. A. Rice, John Wiley & Sons, New York, **1996**, Vol. 94.
3 C. Holm, J. F. Joanny, K. Kremer, R. R. Netz, P. Reineker, C. Seidel, T. A. Vilgis, R. G. Winkler, *Polyelectrolytes with Defined Molecular Architecture II* in *Advances in Polymer Science*, ed. by M. Schmidt, Springer, Berlin, **2004**, Vol. 166, p. 67. doi:10.1007/b10951
4 A. V. Dobrynin, M. Rubinstein, *Prog. Polym. Sci.* **2005**, *30*, 1049.
5 P. G. de Gennes, *Scaling Concepts in Polymer Physics*, Ithaca, Cornell Univ. Press, **1980**.
6 S. A. Safran, *Statistical Thermodynamics of Surfaces, Interfaces, and Membranes*, Westview Press, **2003**.
7 J. N. Israelachvili, *Intermolecular and Surface Forces*, Academic Press, London, **1991**.
8 Y. Marcus, *Ion Solvation*, Wiley, New York, **1985**.
9 V. Gutmann, *The Donor–Acceptor Approach to Molecular Interactions*, Plenum, New York, **1978**.
10 D. Chandler, *Nature* **2005**, *437*, 640.
11 E. L. Eckfeldt, W. W. Lucasse, *J. Phys. Chem.* **1943**, *47*, 164; B. J. Hales, G. L. Bertrand, L. G. Hepler, *J. Phys. Chem.* **1966**, *70*, 3970.
12 V. Balevicius, H. Fuess, *Phys. Chem. Chem. Phys.* **1999**, *1*, 1507.
13 T. Narayanan, A. Kumar, *Phys. Rep.* **1994**, *249*, 135.
14 J. Jacob, A. Kumar, S. Asokan, D. Sen, R. Chitra, S. Mazumder, *Chem. Phys. Lett.* **1999**, *304*, 180.
15 M. Misawa, K. Yoshida, K. Maruyama, H. Munemura, Y. Hosokawa, *J. Phys. Chem. Solids* **1999**, *60*, 1301.
16 M. A. Anisimov, J. Jacob, A. Kumar, V. A. Agayan, J. V. Sengers, *Phys. Rev. Lett.* **2000**, *85*, 2336.
17 T. Takamuku, A. Yamaguchi, D. Matsuo, M. Tabata, M. Kumamoto, J. Nishimoto, K. Yoshida, T. Yamaguchi, M. Nagao, T. Otomo, T. Adachi, *J. Phys. Chem. B* **2001**, *105*, 6236.
18 T. Arakawa, S. N. Timasheff, *Biochemistry* **1984**, *23*, 5912.
19 S. N. Timasheff, *Proc. Natl. Acad. Sci. U.S.A.* **2002**, *99*, 9721.
20 V. M. Nabutovskii, N. A. Nemov, Y. G. Peisakhovich, *Phys. Lett. A* **1980**, *79*, 98.
21 V. M. Nabutovskii, N. A. Nemov, Y. G. Peisakhovich, *Mol. Phys.* **1985**, *54*, 979.
22 A. Onuki, H. Kitamura, *J. Chem. Phys.* **2004**, *121*, 3143.
23 A. Onuki, *Phys. Rev. E: Stat., Nonlinear, Soft Matter Phys.* **2006**, *73*, 021506.
24 A. Onuki, *J. Chem. Phys.* **2008**, *128*, 224704.
25 G. Marcus, S. Samin, Y. Tsori, *J. Chem. Phys.* **2008**, *129*, 061101.
26 M. Bier, J. Zwanikken, R. van Roij, *Phys. Rev. Lett.* **2008**, *101*, 046104.
27 J. Zwanikken, J. de Graaf, M. Bier, R. van Roij, *J. Phys.: Condens. Matter* **2008**, *20*, 494238.
28 D. Ben-Yaakov, D. Andelman, D. Harries, R. Podgornik, *J. Phys. Chem. B* **2009**, *113*, 6001.
29 T. Araki, A. Onuki, *J. Phys.: Condens. Matter* **2009**, *21*, 424116.
30 A. Onuki, T. Araki, R. Okamoto, *J. Phys.: Condens. Matter.*, to be published.
31 B. Rotenberg, I. Pagonabarraga, D. Frenkel, *Faraday Discuss.* **2010**, *144*, 223.
32 R. Okamoto, A. Onuki, *Phys. Rev. E: Stat., Nonlinear, Soft Matter Phys.* **2010**, *82*, 051501.
33 A. Onuki, R. Okamoto, *J. Phys. Chem. B* **2009**, *113*, 3988.
34 R. Okamoto, A. Onuki, *J. Chem. Phys.* **2009**, *131*, 094905.
35 A. Onuki, *Europhys. Lett.* **2008**, *82*, 58002.
36 A. Onuki, *Phase Transition Dynamics*, Cambridge University Press, Cambridge, **2002**.
37 J. D. Reid, O. R. Melroy, R. P. Buck, *J. Electroanal. Chem. Interfacial Electrochem.* **1983**, *147*, 71.
38 G. Luo, S. Malkova, J. Yoon, D. G. Schultz, B. Lin, M. Meron, I. Benjamin, P. Vanysek, M. L. Schlossman, *Science* **2006**, *311*, 216.
39 K. Sadakane, H. Seto, H. Endo, M. Shibayama, *J. Phys. Soc. Jpn.* **2007**, *76*, 113602.
40 K. Sadakane, N. Iguchi, M. Nagao, H. Endo, Y. B. Melnichenko, H. Seto, *Soft Matter* **2011**, *7*, 1334.
41 K. Sadakane, A. Onuki, K. Nishida, S. Koizumi, H. Seto, *Phys. Rev. Lett.* **2009**, *103*, 167803.
42 K. Aoki, M. Li, J. Chen, T. Nishiumi, *Electrochem. Commun.* **2009**, *11*, 239.
43 K. Wojciechowski, M. Kucharek, *J. Phys. Chem. B* **2009**, *113*, 13457.
44 G. W. Euliss, C. M. Sorensen, *J. Chem. Phys.* **1984**, *80*, 4767.
45 Y. Georgalis, A. M. Kierzek, W. Saenger, *J. Phys. Chem. B* **2000**, *104*, 3405.
46 A. F. Kostko, M. A. Anisimov, J. V. Sengers, *Phys. Rev. E: Stat., Nonlinear, Soft Matter Phys.* **2004**, *70*, 026118.
47 M. Wagner, O. Stanga, W. Schröer, *Phys. Chem. Chem. Phys.* **2004**, *6*, 580.
48 C. Yang, W. Li, C. Wu, *J. Phys. Chem. B* **2004**, *108*, 11866.
49 M. Sedlák, *J. Phys. Chem. B* **2006**, *110*, 4329; M. Sedlák, *J. Phys. Chem. B* **2006**, *110*, 4339; M. Sedlák, *J. Phys. Chem. B* **2006**, *110*, 13976.

50 F. Jin, J. Ye, L. Hong, H. Lam, C. Wu, *J. Phys. Chem. B* **2007**, *111*, 2255.
51 J. Jacob, M. A. Anisimov, J. V. Sengers, A. Oleinikova, H. Weingärtner, A. Kumar, *Phys. Chem. Chem. Phys.* **2001**, *3*, 829.
52 G. R. Andersen, J. C. Wheeler, *J. Chem. Phys.* **1978**, *69*, 2082.
53 R. E. Goldstein, *J. Chem. Phys.* **1984**, *80*, 5340.
54 A. Matsuyama, F. Tanaka, *Phys. Rev. Lett.* **1990**, *65*, 341.
55 S. Bekiranov, R. Bruinsma, P. Pincus, *Phys. Rev. E: Stat. Phys., Plasmas, Fluids, Relat. Interdiscip. Top.* **1997**, *55*, 577.
56 J. L. Tveekrem, D. T. Jacobs, *Phys. Rev. A* **1983**, *27*, 2773.
57 D. Beaglehole, *J. Phys. Chem.* **1983**, *87*, 4749.
58 T. Hashimoto, M. Itakura, N. Shimidzu, *J. Chem. Phys.* **1986**, *85*, 6773.
59 P. G. de Gennes, C. Taupin, *J. Phys. Chem.* **1982**, *86*, 2294.
60 E. Raphael, J.-F. Joanny, *Europhys. Lett.* **1990**, *13*, 623.
61 I. Borukhov, D. Andelman, H. Orland, *Europhys. Lett.* **1995**, *32*, 499.
62 I. Borukhov, D. Andelman, R. Borrega, M. Cloitre, L. Leibler, H. Orland, *J. Phys. Chem. B* **2000**, *104*, 11027.
63 P. G. Arscott, C. Ma, J. R. Wenner, V. A. Bloomfield, *Biopolymers* **1995**, *36*, 345.
64 A. Hultgren, D. C. Rau, *Biochemistry* **2004**, *43*, 8272.
65 C. Stanley, D. C. Rau, *Biophys. J.* **2006**, *91*, 912.
66 D. N. Shin, J. W. Wijnen, J. B. F. N. Engberts, A. Wakisaka, *J. Phys. Chem. B* **2002**, *106*, 6014.
67 A. Wakisaka, S. Mochizuki, H. Kobara, *J. Solution Chem.* **2004**, *33*, 721.
68 T. Osakai, K. Ebina, *J. Phys. Chem. B* **1998**, *102*, 5691.
69 T. Osakai, M. Hoshino, M. Izumi, M. Kawakami, K. Akasaka, *J. Phys. Chem. B* **2000**, *104*, 12021.
70 S. Garde, G. Hummer, A. E. Garcia, M. E. Paulaitis, L. R. Pratt, *Phys. Rev. Lett.* **1996**, *77*, 4966.
71 P. R. ten Wolde, D. Chandler, *Proc. Natl. Acad. Sci. U.S.A.* **2002**, *99*, 6539.
72 M. Born, *Z. Phys. A: Hadrons Nucl.* **1920**, *1*, 45.
73 Y. Marcus, *Chem. Rev.* **1988**, *88*, 1475.
74 C. H. Hamann, A. Hamnett, W. Vielstich, *Electrochemistry*, Wiley-VCH, Weinheim, **1998**.
75 L. Q. Hung, *J. Electroanal. Chem. Interfacial Electrochem.* **1980**, *115*, 159; L. Q. Hung, *J. Electroanal. Chem. Interfacial Electrochem.* **1983**, *149*, 1.
76 J. Koryta, *Electrochim. Acta* **1984**, *29*, 445.
77 A. Sabela, V. Mareček, Z. Samec, R. Fuoco, *Electrochim. Acta* **1992**, *37*, 231.
78 L. Degrève, F. M. Mazzé, *Mol. Phys.* **2003**, *101*, 1443.
79 A. A. Chen, R. V. Pappu, *J. Phys. Chem. B* **2007**, *111*, 6469.
80 L. Onsager, N. N. T. Samaras, *J. Chem. Phys.* **1934**, *2*, 528.
81 Y. Levin, J. E. Flores-Mena, *Europhys. Lett.* **2001**, *56*, 187.
82 P. Debye, K. Kleboth, *J. Chem. Phys.* **1965**, *42*, 3155.
83 K. Tojo, A. Furukawa, T. Araki, A. Onuki, *Eur. Phys. J. E* **2009**, *30*, 55.
84 A. A. Aerov, A. R. Khokhlov, I. I. Potemkin, *J. Phys. Chem. B* **2007**, *111*, 3462; A. A. Aerov, A. R. Khokhlov, I. I. Potemkin, *J. Phys. Chem. B* **2007**, *111*, 10189.
85 B. L. Bhargava, M. L. Klein, *Mol. Phys.* **2009**, *107*, 393.
86 P. G. de Gennes, *J. Phys., Lett.* **1976**, *37*, 59.
87 P. K. Weissenborn, R. J. Pugh, *J. Colloid Interface Sci.* **1996**, *184*, 550.
88 A. P. dos Santos, Y. Levin, *J. Chem. Phys.* **2010**, *133*, 154107.
89 J. W. Gibbs, *The Collected Works of J. Willard Gibbs*, Yale University Press, New Haven, CT, **1957**, Vol. 1, pp. 219–331.
90 A. L. Nichols, L. R. Pratt, *J. Chem. Phys.* **1984**, *80*, 6225.
91 G. Jones, W. A. Ray, *J. Am. Chem. Soc.* **1937**, *59*, 187; G. Jones, W. A. Ray, *J. Am. Chem. Soc.* **1941**, *63*, 288; G. Jones, W. A. Ray, *J. Am. Chem. Soc.* **1941**, *63*, 3262.
92 M. Seul, D. Andelman, *Science* **1995**, *267*, 476.
93 V. Y. Boryu, I. Y. Erukhimovich, *Macromolecules* **1988**, *21*, 3240.
94 J. F. Joanny, L. Leibler, *J. Phys. France* **1990**, *51*, 547.
95 O. Braun, F. Boue, F. Candau, *Eur. Phys. J. E* **2002**, *7*, 141.
96 I. F. Hakem, J. Lal, *Europhys. Lett.* **2003**, *64*, 204.
97 I. F. Hakem, J. Lal, M. Bockstaller, *Macromolecules* **2004**, *37*, 8431.
98 A.-C. Shi, J. Noolandi, *Macromol. Theory Simul.* **1999**, *8*, 214.
99 Q. Wang, T. Taniguchi, G. H. Fredrickson, *J. Phys. Chem. B* **2004**, *108*, 6733; Q. Wang, T. Taniguchi, G. H. Fredrickson, *J. Phys. Chem. B* **2005**, *109*, 9855.
100 N. Ise, T. Okubo, S. Kunugi, H. Matsuoka, K. Yamamoto, Y. Ishii, *J. Chem. Phys.* **1984**, *81*, 3294.
101 B. D. Ermi, E. J. Amis, *Macromolecules* **1998**, *31*, 7378.
102 J. Zhou, A.-C. Shi, *J. Chem. Phys.* **2009**, *130*, 234904.
103 S. A. Patel, C. L. Brooks, III, *J. Chem. Phys.* **2006**, *124*, 204706.

Akira Onuki was born in Hokkaido, Japan, in 1948. He received Ph.D. degrees from the University of Tokyo in 1976 under the supervision of Prof. Ryogo Kubo. After one year as JSPS fellow, he was Assistant Professor at Physics Department of Kyusyu University (1977–1983) and worked with Prof. Kyozi Kawasaki. He then moved to Kyoto University as Associate Professor at Yukawa Institute (1983–1991) and as Professor at Physics Department (1991–). He has studied mainly phase transition dynamics and soft matter physics. He produced first theoretical papers on shear flow effects in near-critical fluids, adiabatic effects in compressible fluids, elastic effects in phase separation in metallurgy, heat flow effects near the superfluid transition, viscoelastic effects in polymers, and collective effects in glass dynamics. He published a book, "Phase Transition Dynamics", from Cambridge University Press (2002). His current interests are on heterogeneous glass dynamics, dynamic van der Waals theory, and solvation effects. He received Nishinomiya Yukawa prize in 1989.

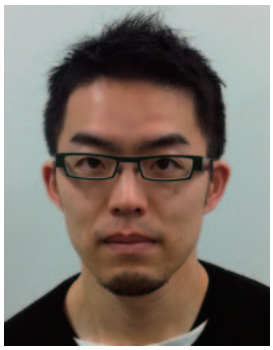

Ryuichi Okamoto was born in Gifu, Japan, in 1980. He received Ph.D. from Keio University in 2007 under the supervision of Prof. Youhei Fujitani. He has been a postdoctoral fellow with Prof. Akira Onuki at Kyoto University since 2007. His current research focuses on the solvation effects in soft matter physics from a mesoscopic view point.

Takeaki Araki was born in Nagasaki, Japan, in 1972. After he graduated from the University of Tokyo in 1991, he worked with Prof. Hajime Tanaka as technical associate. He became Assistant Professor in 2001, and he then moved to Kyoto University as Associate Professor in 2008. He recieved Ph.D. (Engineering) from the University of Tokyo in 2003. His reseach interests maily focus on phase transition dynamics in soft matters. He recieved Young Scientist Award of the Physical Society of Japan in 2007, and The Young Scientists' Prize from The Commendation for Science and Technology by the Minister of Education, Culture, Sports, Science and Technology in 2009.